



Multi-tool dataset on Northern Eurasian Riverbank Migration (NERM)

Sergey R. Chalov¹, Victor Ivanov¹, Danila Shkolnyi¹, Ekaterina Pavlyukevich^{1,2}, Michal Habel³, Dmitry Botavin¹, Aleksandra Chalova¹, Pavel Golovlev¹, Arseny Kamyshev¹, Roman Kolesnikov⁵, Uliana Koneva¹, Anna Kurakova¹, Nadezda Mikhailova¹, Elizaveta Tuzova¹, Kristina Prokopeva^{1,2}, Aleksandr Zavadsky¹, Rituparna Acharyya³, Roman S. Chalov¹, Aleksandr Varenov⁴, Leonid Turykin¹, Anna Tarbeeva¹, Daidu Fan⁶

¹Lomonosov Moscow State University, Moscow, 119991, Russia

²Water Problems Institute of RAS, Moscow, 119333, Russia

10 ³Uniwersytet Kazimierza Wielkiego, Bydgoszcz, 85-033, Poland

⁴Minin Nizhny Novgorod State Pedagogical University, Nizhny Novgorod, 603005, Russia

⁵Arctic Research Center of the Yamal-Nenets Autonomous District, Salekhard, 629008, Russia

⁶Tongji University, Shanghai, 200092, China

15 *Correspondence to:* Ekaterina Pavlyukevich (ekaterina.kornilova.hydro@gmail.com)

Abstract. Riverbank erosion monitoring and modeling has a long-standing tradition in Earth system science. The current body of research primarily relies on observations at the basin and reach levels. We endeavored to compile a comprehensive dataset of riverbank migration observations using a variety of measurement techniques, both field-based and remote sensing data. The dataset comprises information from twelve extensive river basins situated in Northern Eurasia, encompassing rivers that drain into the Baltic Sea, the Arctic and Pacific Oceans, and the Caspian Sea, specifically the catchments of the Vistula, Volga, Ural, Ob, Nadym, Yenisey, Lena, Indigirka, Yana, Kolyma, Amur and Kamchatka rivers. The rivers included in the dataset vary in terms of environmental conditions and have average discharges of between 0.3 and 19,700 m³/s. This study examined approximately 140,000 kilometers of rivers in Northern Eurasia, covering small, medium, and large rivers, with data from up to 70 years of water classifications obtained from satellite images, including those from LandSat and Keyhole, across 626,700 river channel segments. The dataset collected average and maximum bank retreat rates (m/year), average areas of bank retreat (m²/year), and volumes of channel erosion (t/year). It also recorded possible causes, encompassing both hydrological and catchment factors like permafrost, natural land zones, and geology. Our study showed that river discharge and permafrost distribution are the primary indicators of riverbank erosion in Northern Eurasia. These data will enhance the comprehension of bank erosion processes and their underlying factors, thereby facilitating the development of more accurate predictive models of river channels. The dataset is available open access via the ZENODO repository (<https://doi.org/10.5281/zenodo.11072919>) (Chalov et al., 2025).



1 Introduction

Approximately 2.5 billion individuals globally reside near major rivers and utilise them for water supply, transportation, and power generation (Musie and Gonfa, 2023). Characteristics of rivers change over time and in different locations, as noted in
35 (Knighton, 2014) and (Bracken et al., 2015). Specifically, alterations in their spatial limits are associated with hydromorphological processes occurring at various spatial scales, such as bank-scale, reach-scale, and floodplain-scale, and involve vertical and horizontal modifications of river channels (Alabyan and Chalov, 1998). The latter results in the most hazardous river-related phenomena, specifically lateral (riverbank) erosion, which leads to land loss and the conversion of floodplains into active channels.

40 Riverbank erosion has long been viewed as a threat to structures, engineering projects, infrastructure, and agricultural operations. This phenomenon can significantly contribute to sediment loads in rivers, thus serving as a crucial factor in sediment flux models (Kronvang et al., 2013; Wilkinson et al., 2009). Long-lasting effects on riverbank migration are caused by both natural and man-made changes to water and sediment supply, with the river's channel shape adjusting to new conditions (Alexeevsky et al., 2013; Brandt, 2000). Riverbanks serve as both a source (by erosion) and reservoir (by deposition on them)
45 for sediment, highlighting the effects of fluctuating sediment supply (Kronvang et al., 2013). Furthermore, chemicals such as metals and carbon stored in riverbank sediments are transported downstream to coastal seas due to bank deterioration (Reid and Dunne, 2016), in some cases significantly impacting terrestrial flux (Chalov and Ivanov, 2023; Chalov et al., 2023b; Gautier et al., 2021).

Researchers globally have investigated river planform transformations over the course of time to identify evolutionary patterns,
50 evaluate influencing factors, and control the fluvial ecosystem, which has led to a variety of measurement techniques. Laboratory flume experiments and detailed field measurements with erosion pins have validated methods for measuring river movement at reach scales (Guy et al., 1966; Thorne, 1981). The conventional method of measuring bank erosion involves a thorough historical examination of riverbeds, taking into account available cartographic records and aerial images to evaluate changes in the river's shape (Fuller et al., 2003; Mandarino et al., 2019), which encompasses georeferencing of images,
55 interpreting photos, digitizing morphological features, and performing vector and raster geospatial analysis. Remote sensing data, including repeated LiDAR and optical remote sensing, notably improves the ability to track channel dynamics over large spatial areas and at decadal time intervals. These methods are based on retreat area detection, which involves assessing the movement of rivers by observing how channelized areas and regions without channels (like floodplains) evolve over time (Langhorst and Pavelsky, 2023). Comparisons of satellite images are used to create bank retreat polygons (Kurakova and
60 Chalov, 2019) or centerlines (Greenberg et al., 2023). Current methods of measuring river mobility through remote sensing focus mainly on meandering rivers with a single channel, and primarily emphasize bank movement (Donovan and Belmont, 2019; Sylvester et al., 2019). Furthermore, recent techniques like particle image velocimetry (PIV) (Chadwick et al., 2023) are being extensively utilized for monitoring bank erosion.



65 Studies on bank erosion are crucial, yet data on this topic are scarce due to the high expense of collecting and interpreting
them, and available data are mostly confined to specific river sections and watersheds. Datasets employed in riverbank erosion
research include the GSWE – Global Surface Water Explorer, which uses a supervised classification of Landsat-5, -7, and -8
satellite imagery from 1984 to the present (Pekel et al., 2016), as well as the GLAD dataset, wherein water surface was
calibrated with RapidEye imagery (Pickens et al., 2020). Global datasets designed to compile a consistent record of riverbank
migration worldwide have been introduced by (Ielpi and Lapôtre, 2020), utilizing a sample of 983 meanders, and by (Langhorst
70 and Pavelsky, 2023), who created REAL (Riverbank Erosion and Accretion from Landsat) – a global dataset of riverbank
erosion covering over 370,000 km of major rivers, based on GSWE and GLAD data.

These datasets are restricted to decadal-scale average riverbank erosion and rivers with widths exceeding 150 m, whilst also
concentrating solely on the surface water occurrence dataset obtained from Landsat satellite imagery; as a result, more
extensive observations of contemporary riverbank erosion rates are needed, encompassing different methods and rivers. In
75 Northern Eurasia, it is notably significant that nearly a quarter (about 26%) of areas with extremal bank erosion are recorded
in the Langhorst and Pavelsky database (2023).

Recent studies on riverbank migration have been conducted for the biggest rivers in Northern Eurasia as part of international
collaborative projects (Babiński et al., 2014; Lappalainen et al., 2018). Results of these studies, with rare exceptions
(Alexeevskii et al., 2008; Alexeevsky et al., 2013), was not accessible to the international scientific community. The current
80 work enables the presentation of a multi-tool dataset of channel erosion rates encompasses rivers within the major catchments
in Northern Eurasia, covering a total length of more than 140,000 km of river networks, also presented as an online GIS map
(<https://map.giscarta.com/viewer/93a6a4b3-179f-450f-be02-a31ca6db245b>).

The purpose of this research is to provide a multi-scale dataset featuring outputs from the use of multiple tools to identify
changes in planform at various scales, encompassing extreme values of bend migration at localized spots, estimates with a
85 spatial resolution of 10 to 100 m at the reach scale, and basin-scale averages with 1 km resolution. Following the dataset
attributes description, we present a comparative analysis of contemporary riverbank erosion rates across different catchments
and river sizes. We examine extreme variations in river channel changes across the entire dataset, focusing on large catchments
such as the Ob River and specific environments like the Lena River delta, as well as long-term changes of bank erosion rates.
The study of the dataset illustrates how it can be employed to calculate the in-channel contribution to sediment transport.

90 **2 Material and methods**

2.1 Rivers

This paper presents a dataset compiled from field-based observations and satellite images, including LandSat and Keyhole,
that spans over 140,000 km of riverbanks in Northern Eurasia. The dataset covers small, medium, and large rivers and was
compiled using different methods of image classification and digitization from bank transitions acquired over a 60-year
95 interval. The dataset comprises more than 626,000 river channel reaches, as detailed in Table 1, covering rivers belonging to



the watersheds of the Baltic Sea, Arctic and Pacific Ocean, and Caspian Sea. In total, over 250 rivers were examined across 28 distinct subdatasets, each of which focuses on a separate river section, or a group of rivers with similar landscape characteristics, or the largest rivers within a major watershed, or deltas as distinct distributary systems (Table 1). Each subdataset was derived through one of the methods detailed below and was identified by a unique ID within the dataset, ranging from 1 to 28. The compiled data were employed in both statistical and qualitative examinations. The river distribution allows for the identification of the impacts of geology, hydrology, permafrost and vegetation by assigning each river to successive categories.

Table 1. Description of rivers included in the dataset

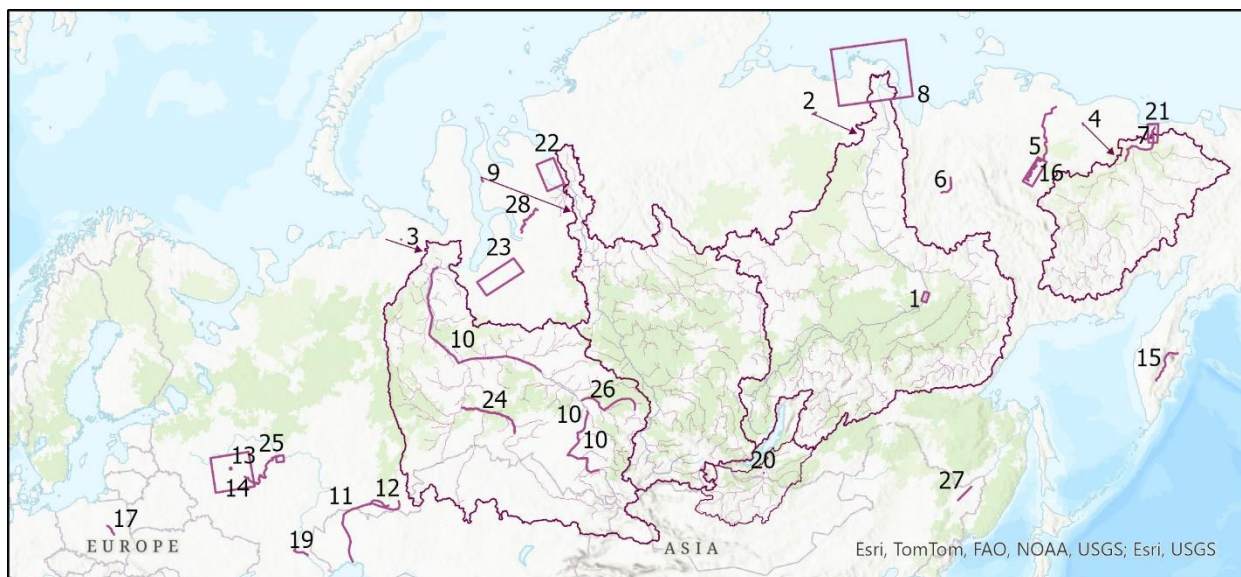
ID	River	Catchment	L, km	B_{mean} , m/year	B_{max} , m/year	Q, m ³ /s	Temporal range
1	Lena, Yakutsk	Lena	1750	2.6	23.8	7272 - 7297	1965–1993
2	Rivers of the Lena river basin	Lena	34 800	0.8	14.6	30 - 15701	1986–2021
3	Rivers of the Ob river basin	Ob	30 200	0.5	7.67	30 - 13498	1985–2021
4	Rivers of the Kolyma river basin	Kolyma	8 100	0.81	8.84	30 - 3718	1999–2021
5	Indigirka	Indigirka	618	1.31	23.9	913-1,780	2000–2019
6	Yana	Yana	225	1.42	8.3	154-182	2002–2021
7	Kolyma	Kolyma	400	1.50	13.0	2,350-3,720	1965–2021
8	Lena, delta	Lena	14 600	0.89	5.99	15,800	2000–2021
9	Rivers of the Yenisey river basin	Yenisey	34 800	0.55	9.02	30 - 19744	1985–2019
10	Ob	Ob	4 000	1.67	26.3	1,040-13,400	1968–2022
11	Ural	Ural	1 700	2.18	20.9	64-337	1985–2015
12	Sakmara	Ural	330	1.90	8.3	44-250	1985–2015
13	Setun and Ramenka	Volga	20	0.15	0.62	1-2.4	1942–2010
14	Rivers of Moscow region	Volga	60	0.18	1.3	0.5-490	2003–2010
15	Kamchatka	Kamchatka	320	1.08	15.8	64-904	1967–2017
16	Indigirka	Indigirka	260	1.42	7.45	913-1,500	1975–2017
17	Vistula	Vistula	120	8.81	50.7	1,080-1,080	2006–2023
18	Rivers of the Kudma river basin	Volga	30	0.2	0.13	0.3-6.7	2017–2023
19	Volga	Volga	230	6.75	53	8,200-8,240	1977–2022
20	Rivers of the Selenga river basin	Yenisey	8 617	0.95	6.29	1-2,450	1984–2016
21	Yenisey delta	Yenisey	200	0.98	5.69	19,700	2000–2022
22	Kolyma delta	Kolyma	120	1.11	3.04	3,700	2001–2022
23	Rivers of Yamal region	Pur, Nadym	2	1.2	2.5	5-10	2022–2024



24	Irtysch	Ob	1 690	2.38	20.9	930-2,920	1985–2021
25	Oka	Volga	805	1.1	10.2	560-1,330	2002–2022
26	Chulyum	Ob	1 100	1.69	13.2	240-780	2002–2022
27	Ussuri	Amur	214	1.06	8.5	210-820	2002–2022
28	Messoyakha	Messoyakha	296	2.17	14.5	100-310	1976–2023

105 Explanations: L – length of subdataset river sections [km]; B_{mean} – average bank retreat rates [m/year]; B_{max} – maximum bank retreat value [m/year]; A_{mean} – average area of bank retreat [m^2/year]; Q_{mean} – annual mean river water runoff [m^3/s] (Lehner, Grill, 2013).

The rivers presented in the dataset present contrasting conditions (Fig. 1) of channel erosion. The Vistula River (#17) case study reach extends over 120 km of the middle section of the Vistula River, between the mouth of the Radomka River and the Narew River (km 430-551 of waterway). This section is partially trained by transverse and longitudinal river groins (medium-
 110 water-level riverbed) and flood embankments (high-water-level riverbed). In the urban section, the riverbed is strongly confined, having been narrowed to embankments (e.g., in Warsaw), and incised (Bujakowski and Falkowski, 2019).



ID River

- 1 Lena, Yakutsk
- 2 Rivers of the Lena river basin
- 3 Rivers of the Ob river basin
- 4 Rivers of the Kolyma river basin
- 5 Indigirka
- 6 Yana
- 7 Kolyma, 300 km downstream + delta

ID River

- 8 Lena delta
- 9 Rivers of the Yenisej river basin
- 10 Ob
- 11 Ural
- 12 Sakmara
- 13 Setun and Ramenka
- 14 Moscow region rivers

ID River

- 15 Kamchatka
- 16 Indigirka
- 17 Vistula
- 18 Kudma catchment
- 19 Volga
- 20 Selenga
- 21 Kolyma delta

ID River

- 22 Yenisey delta
- 23 Yamal peninsula rivers
- 24 Irtysch
- 25 Oka
- 26 Chulyum
- 27 Ussuri
- 28 Messoyakha

Figure 1. Locations of river sections included in the dataset

115 The Volga River's largest right tributary, the Oka River (#25), is a vital waterway in the East European Plain, where a dense population has led to substantial human-induced pressure and notable changes in water and channel conditions. Sand mining



in riverbed quarries is a highly influential activity that can significantly impact the stability of a channel (Berkovich, Zlotina and Turykin 2023). The Oka River has a total length of 1500 km, with 805 km of that distance located in the middle and lower parts between the confluence points of the Moskva and Klyazma rivers and included in the dataset. Here, Oka's course winds through a primarily expansive floodplain. Additionally, data of the 230 km of the downstream Volga River (#19) between
120 Volgograd and Astrakhan cities is included in the dataset. Here, the river flows through the steppe zone, and closer to the south its banks are conquered by semi-desert, and is characterized by alluvial sandy channel. Here the dam located at Volgograd significantly influences hydrological regime both by decreasing average and maximal discharges, water levels lowering, and a release wave passage when water level variation immediately downstream the dam can reach 2.5 m day⁻¹.

Small rivers located in the Moscow region (#14), including a few rivers within Moscow City (#13) and rivers in the central
125 part of the Nizhny Novgorod region (#18), are also located within the Volga Basin. In the Nizhny Novgorod region, the case study includes the Kudma River and its tributaries – the Ozerka, Setchuga and Pechet' Rivers. The Kudma River is a right tributary of the Volga River downstream of the confluence with the Oka River. The total length of the river is 144 km. The Ozerka River, which is 74 km long, is the largest tributary of the Kudma River. Setchuga and Pechet' are small tributaries of the Kudma and Ozerka Rivers, respectively.

130 The Setun River (#13) is the largest right tributary of the Moskva River within Moscow City. It flows into the Moskva River at 174 km from its mouth. The total length of the river is 38 km. Eighteen kilometers from its confluence with Moskva, it crosses the Moscow Ring Road and then flows through the city. Its main tributary is the Ramenka River (#13), which is also included in the dataset.

The Ural River (#11) and its principal tributary, the Sakmara (#12), form the border between Europe and Asia and flows
135 through parts of Russia and Kazakhstan. Ural is currently the only major river that flows freely into the Caspian Sea. Channel erosion within the Ural catchment has been the focus of relatively few studies (Yarushina et al. 2009; Sergaliev and Akhmedenov 2014), which propose relatively high values in comparison to nearby rivers, primarily attributed to the river's course through a vast steppe region.

Approximately 4000 km of the primary course of the Ob River (#10) were incorporated into the dataset. The Ob River is
140 situated within the West Siberian Plain, where the geological and geomorphological conditions are relatively uniform. The floodplain and terraces are comprised of alluvial deposits, including sand, sandy clay, and light loam. This results in active riverbank erosion. The bedrock of the Ob River, predominantly found in its lower course, typically comprises solid loamy sediment deposits (Kurakova and Chalov, 2019). The two longest tributaries of the Ob are also part of the dataset. Lower reaches of the Irtysh (#24), a key transboundary river, has been added to the dataset, specifically the section between the
145 Russian-Kazakh border and its mouth. The river's meandering channel has evolved over the past decades under low water conditions, partly due to the regulation of its upper sections by reservoirs. The second longest tributary of the Ob, Chulym (#26), has the lower reach section included, 1100 km upstream from its mouth to the city of Achinsk, where it originates from the low-lying Arga Ridge and extends into the plain, subsequently meandering through a vast floodplain that is flanked by



150 taiga forests and bogs. Furthermore, more than 220,000 bank erosion sections with total length of 30,200 km of all rivers in the Ob Basin (#3) and annual discharge values of at least 30 m³/sec were studied.

The adjacent tundra-taiga areas of the low plains are located east of the Ob mouth area. Here, rivers are formed in broad sandy alluvial deposits composed of marine loam and alluvial sands (Sidorchuk, 2019). With the seasonally thawed layer reaching about 2 m deep in the area, this area is one of the most severely gullied landscapes in the Russian Arctic, with a gully density of up to 1–2 km/km² and a very unstable channel. Three sites of channel monitoring were established in 2022 at the small and medium Sedayakha, Tyjakha and Khaduta Rivers (#23). The largest river of the Gydan Peninsula, the Messoyakha (#28), was also included in the base from the confluence with the Nyangus-Yakha River to the head of the delta. It flows under similar conditions, but has a much higher flow rate, and its channel processes are regulated by the active change of base level due to the growth of the river delta in the Holocene. Through this process, the rates of horizontal deformations on the river are much higher than typical for this natural zone.

160 The low plains' adjacent tundra-taiga regions are situated east of the Ob river mouth area. Rivers originate in expansive sandy alluvial deposits consisting of marine loam and alluvial sands (Sidorchuk, 2019). With the seasonally thawed layer reaching about 2 m deep in the area, this area is one of the most severely gullied landscapes in the Russian Arctic, with a gully density of up to 1–2 km/km², and rivers here have a very unstable channels. Channel monitoring sites were set up in 2022 at the Sedayakha, Tyjakha, and Khaduta Rivers, which are small to medium in size (#23). The Messoyakha (#28), which is the largest river of the Gydan Peninsula, was also included in the dataset from the confluence with the Nyangus-Yakha River to the head of its delta. Under similar circumstances, it has a much greater flow rate, and the river channel's processes are managed by the shifting base level resulting from the expansion of the river delta during the Holocene period. This process results in significantly higher rates of horizontal deformation along the river than would be particularly expected in this natural region. 34 800 km of rivers of the Yenisey Basin (#9) were analyzed, this subdataset consists of 98542 eroded sections of all rivers of the Yenisey Basin that exceed the value of annual discharge of 30 m³/sec. The Yenisei River and its tributaries have mainly incised relatively straight channels with occasional braided sections and meanders, which are related to the geological structure of its valley. The banks of this river are composed of massive crystal rocks of Permo-Triassic origin (Saunders et al., 2005). The delta of the Yenisey River (#21) is 50 km wide and 200 km long. The present study considers over 200 km of the Yenisey Delta distributary channels.

175 The Selenga River Basin (#20) is the largest tributary of Lake Baikal and belongs hydrographically to the Yenisey River catchment. The Selenga River is situated between the mountain systems of Southern Siberia (Sayan, Khangai) and the plains of central Mongolia, draining both southern taiga, forest-steppe, steppe and semi-desert. In the Selenga Basin, there are a wide variety of geological and geomorphological conditions for the origin of different types of channels, from wide floodplains to incised ones. The total length of channels of rivers of the Selenga Basin, which was considered in this dataset, is 8,617 km.

180 The Ussuri River (#27) is a major right tributary of the Lower Amur, and for much of its length it straddles the border between Russia and China. A significant part of the watershed lies in the Sikhote-Alin Mountains, and the basin includes large Lake



Khanka. A 214 km section of the river (with a total length of 897 km) is presented in the database between the Siniy and Wandashan ranges, where it has an actively meandering channel and flows through the broad, swampy Ussuri plain.

34 800 km of rivers of the Lena Basin (#3) were analyzed, this subdataset consists of 132666 eroded sections of all rivers of the Lena Basin that exceed the value of annual discharge of 30 m³/sec. Geological differences between the riverbeds of the Lena Basin influence the channel processes. The upper reaches of the Lena River, together with the Vitim, Olekma, and incised channels, characterize the upper reaches of the Aldan, and bedrock-controlled erosion and stable channels dominate the Vilyuy, while the middle and lower reaches of the Lena River experience active lateral migration, sediment accumulation, and floodplain development. For example, the Lena River near Yakutsk (#1), that is middle course, is mainly anabranching with sandy sediments. Previous studies on channel migration in catchment areas are maintained in works by (Gautier et al., 2021), which suggest significant rates of bank retreat in this region and the key role of permafrost degradation in channel erosion processes. Additionally, the Lena Delta (#8) is the largest distributary channel pattern in the Arctic region, extending 32,000 km² with 6,000 branches, of which a total 14,600 km is specifically focused on in the dataset. The baseline conditions of channel formation in the Lena River Delta are controlled by river–sea interaction and meteorological factors, as well as past formation features and the continuous presence of permafrost (Chalov et al., 2023a). The largest parts of the ice complex (or yedoma) are located here. Bank erosion estimate covers 90% of the delta terrain, with only 3,300 km² excluded from the analysis. Four main branches were analyzed for the Lena River Delta: the channels of the Bykovskaya (100 km length), Trofimovskaya (120 km), Tumatskaya (140 km) and Olenekskaya (170 km).

The Yana River (#6) is examined in its upper reaches, covering a 225 km stretch from its origin at the confluence of the Dulgalakh and Sartang Rivers to the confluence with the Adycha River, out of the river's total length of 872 km. This area features a meandering channel that occurs in a broad and deep valley situated within the intermountain depression between the foothills of the Yana Plateau. Permafrost comprises the majority of the eroding banks' length, primarily made up of frozen alluvium, which contains distinct separate ice wedges.

Analysis of the Indigirka River (#16, #5) was conducted employing diverse techniques (both manual and automated) over a 618-km segment spanning from the point where the river enters the lowland, characterised by a sudden decrease in channel slope and a transition in channel type from branching to predominantly meandering, to the beginning of the delta. This area is marked by a broad valley dominated by a large floodplain and the first river terrace, complicated by individual water channels with considerable lengths and relatively low water levels.

For the Kolyma Basin, there is dataset (#7) that provides estimates for the 300 km downstream sections of the river system and its estuary. In this area, the Kolyma has a mainly meandering sandy channel with significant outcrops of yedoma sediments with high ice content (Strauss et al., 2021). Sparse evidence suggests (Murton et al., 2015) that channel dynamics have increased over recent years due to the climate-driven collapse of yedoma outcrops. In addition, 8100 km with 113875 eroded sections of all rivers of the Kolyma Basin (#4) that exceed the value of the annual discharge of 30 m³/sec were analyzed. Significantly smaller than the Lena Delta, the Kolyma River Delta (#22) consists of two main branches and is also formed by the accumulation of sediments from the river and from the erosion and abrasion of ancient landforms due to sea-level



fluctuations and tectonic movements of the Earth's crust. The total length of the estimated channel distributary network in the Kolyma Delta is 120 km, covering over 3,200 km² of the delta.

220 The Kamchatka River (#15), located at the easternmost point of the dataset, is the largest river of the Kamchatka peninsula situated in the Russian Far East. The 580 km section that was analysed spans approximately 77% of the total river length, commencing where the river exits the mountains and enters the Central Kamchatka plain, and terminating in a river gorge within the Kumroch range, just before the river's mouth area begins.

2.2 Bank erosion dataset and methods

225 Owing to differences in river sizes and the limitation of the analyses to particular river reaches, the compiled dataset relies on five main tools applied at various spatial levels (Table 2). Compatibility and validation of the tools are discussed in the next section. All methods provided data on bank erosion rates (m/year), whereas area-based approaches provided additional data on the area (m²/year) and volume (m³/year) of bank collapse due to erosion (and mass of sediment release, t/year):

- method I: on-site local measurements based on field-based measurements of bank erosion in a particular reach;
 - methods II, III, IV: linear methods, which are applied for extended river reaches based on tools that track either the banklines (obtained by manual digitizing [method II] or by the application of a specific GIS digitizing algorithm [method IV]) or stream centerlines (method III);
 - method V: area-based approaches, which are based on classifications of water and land from satellite images and further applied to quantify riverbank erosion as transitional pixels from land to the river.
- 230



Table 2. Overview of applied tools

Method	I	II	III	IV	Va	Vb
Applied tools	Manual measurements with geodesic instruments and UAVs	Manual digitizing in ArcGIS	Centerline method in ArcGIS	Digital Shoreline Analysis System (DSAS)	Rstudio, ArcGIS	
					using existing databases	using water indices
Site numbers	14, 18, 23	1, 7, 10, 15, 16, 19, 28	11, 13, 12, 20, 24	17	2, 3, 4, 9	5, 6, 8, 21, 22, 25, 26, 27
Rivers	Moscow region rivers, Kudma catchment rivers, Yamal region rivers	Lena; Kolyma; Ob, Indigirka, Volga, Kamchatka, Messoyakha,	Ural, Sakmara, Setun and Ramenka, Selenga catchment, Irtysh	Vistula	Lena, Ob, Yenisey, Kolyma basins	Yenisey, Lena, Kolyma deltas; Indigirka, Oka, Chulym, Ussuri, Yana
List of parameters in dataset	Bmean, Bmax	Bmean, Bmax, Amean	Bmean	Bmean	Bmean, Amean, Bmax, Vmean	

235

I. On-site local measurements. Measurements taken directly on-site rely on regular surveys of a river's planform, a method suitable for monitoring deformation in small rivers (#14,18). Rods are positioned along the banks, especially those that have eroded, at a certain distance from them to create a grid that spans the area to be mapped. Two tapes were utilised to record data along the transect: one measured the distance between two rods, while the second tape measured the perpendicular distance from the first tape to specific points on the eroded bank (e.g. the top, toe, etc.) at intervals between the rods. The site's bank erosion intensity data could be obtained with a level of accuracy of 1 cm. Orthophotography and a digital elevation model (DEM) surface were also generated annually via UAV-based surveys during field campaigns (Fig. 2), covering the Yamal Peninsula rivers (#23). Estimates of some rivers within Moscow city (such as the Setun, Ramenka, #13) - particularly unaltered and non-channelized sections - were combined with satellite imagery processing. A combination of aerial images from 1942 and Google Earth images from 2010 was made.

240
245

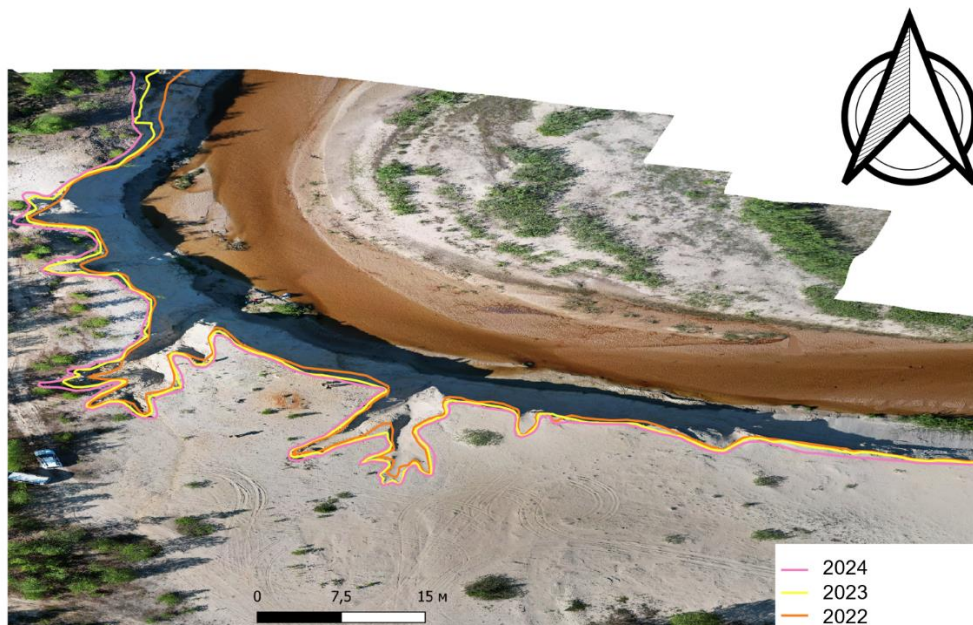
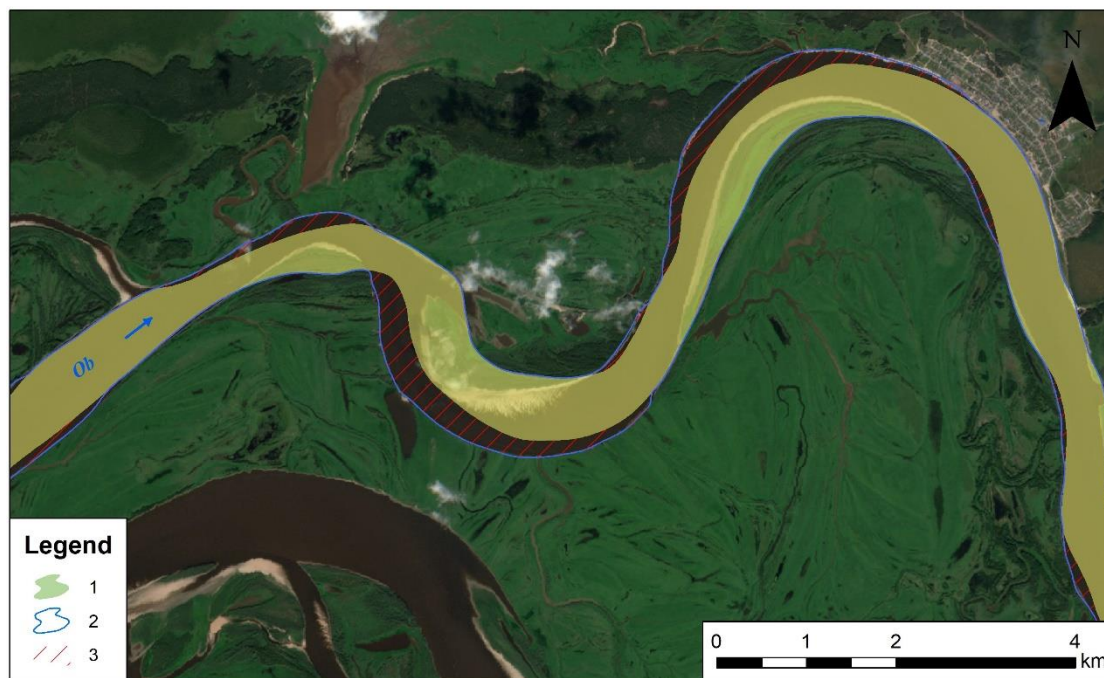


Fig. 2. Location of bankline revealed from UAV at the Tayakha River at Yamal (orange – September 2022; green – August 2023; red – July 2024)

II. Manual digitizing. This method of riverbank migration analyses was undertaken by comparing satellite images captured at times of similar water flow rates (low-water periods in August or September) with a deviation of 5% from standard discharge levels. Satellite images from the CORONA series, which have a resolution of 1.8 m, and those from the Landsat 5 satellite with a 30 m resolution, were chosen as the earliest available images. The current position of the riverbank line was evaluated using multispectral satellite images obtained from Sentinel-2 with a resolution of 10 m and Landsat 7 and 8 with resolutions ranging from 15 to 30 m. The methodology involved comparing the positions of riverbank lines that had been digitized from satellite images taken in various years, as shown in Figure 3. Consequently, we identified riverbank erosion fronts, and used ArcGIS tools to determine the mean and maximum annual erosion rates, as well as the area of erosion. Riverside bank retreats were also calculated using manual image analysis of Keyhole imagery dating back to around 1964-75 and subsequent detailed analysis of Quickbird, Worldview, and Spot satellite images from approximately 2012-18.



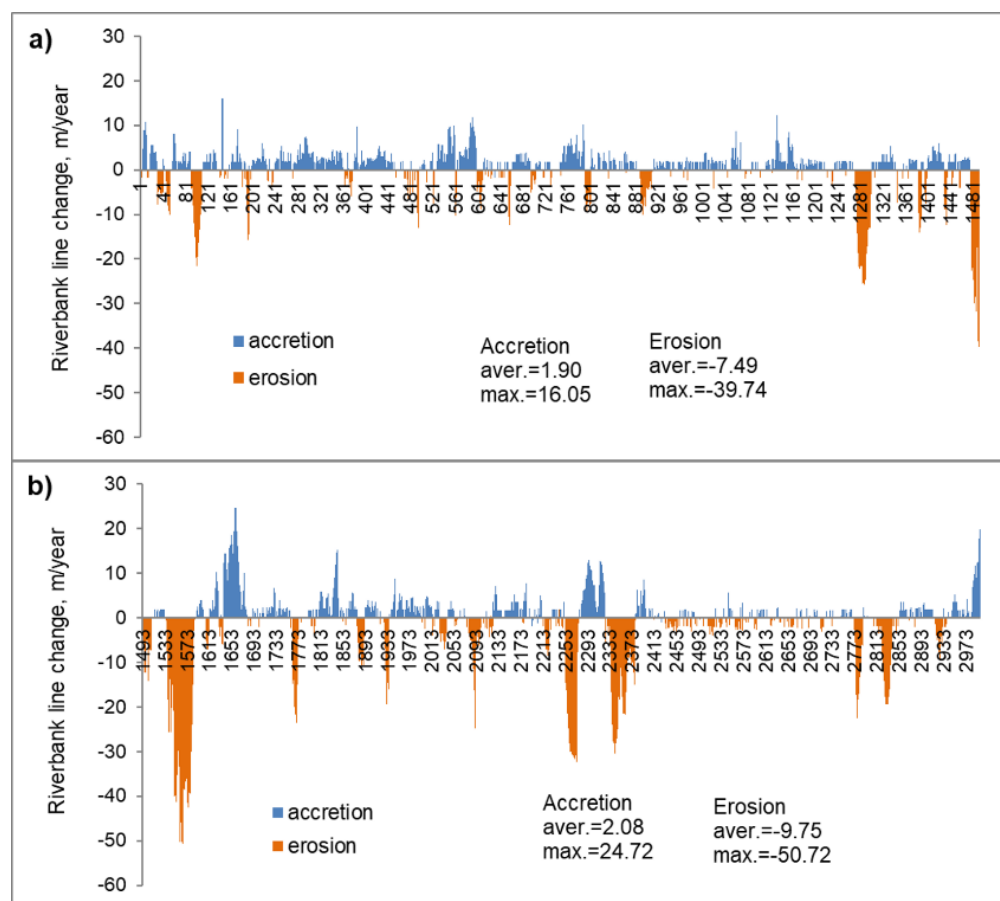
260 **Fig. 3. Comparison of positions of riverbank lines of Ob (#10) middle reach : 1 – 1970 year, 2 – 2018 year, 3 – channel erosion areas (1970–2018) (© Esri Imagery)**

III. Tracking river centerline movement. The method of long-term channel migration was based on river centerline calculation from satellite images in ArcGIS. The methodology was based on the classification of satellite imagery using the *Maximum Likelihood Method*, which involves identifying and digitizing three training sets: a) water surface or fluvial bed; b) island banks, bars, areas without vegetation and sand; c) islands covered by perennial vegetation. These training sets are used to generate a classified raster output for each satellite image. The water surface was automatically extracted from a combination of visible red, NIR, and SWIR channels, and erosion polygons were calculated as the positive difference between the 2019 and 2000 water surface rasters. For each erosion polygon, the centerline was constructed and then smoothed using a Savitzky-Golay linear filter, which allowed the construction of near-parallel transects that were used to parameterize the erosion rate for points every 10 m. This approach was implemented along 8,617 km of rivers in the Selenga Basin (#20), Irtysh (#24), Ural (#11), and Sakmara (#12) rivers.

IV. Digital Shoreline Analysis System (DSAS) in ArcGIS. For some of the case studies, the application of the Digital Shoreline Analysis System (DSAS) was tested based on an automated statistical model deployed to estimate riverbank erosion/accretion along a selected reach of the Vistula River’s middle stream. The DSAS model developed by USGS as a key component of its “Coastal Change Hazards” program calculates a comprehensive array of regression statistics within a systematic, readily repeatable method that can be implemented on a large amount of data (USGS 2019). The DSAS model is operating based on statistical estimation methods to calculate the rate-of-change statistics from satellite data. DSAS calculates erosion and accretion based on a time series of vectorized shoreline positions marked by transects generated from a referenced



baseline (Himmelstoss et al. 2021). In this study, bankline assessment was carried out using two different measurement
 280 calculations: the end-point rate (EPR) and the shoreline change envelope (SCE). The EPR is calculated by dividing the distance
 between two given shorelines by the time elapsed between the oldest and most recent shoreline, whereas SCE reports a distance
 (in meters) and does not document a change rate. In this analysis, the DSAS model was employed in the selected study area,
 utilizing distinct Landsat images of the Vistula River spanning between 2006 and 2023 to quantify riverbank erosion and
 accretion by implementing the following steps (Fig. 4). Thus, the persistent bank line of distinct years (2006 and 2023) was
 285 delineated using Landsat images to assess erosion/accretion via DSAS. The generated binary raster datasets were then
 transformed into vector data, and the land–water boundary was demarcated. DSAS needs a single land–water boundary as
 input, which is called the “baseline”, and the erosion/accretion is calculated relative to the baseline. The baselines created for
 both the right and left banks had a buffer of 200 m, and the transects were cast perpendicular to the baseline at intervals of 100
 m (Fig. 4).



290

Fig. 4. Endpoint Rates (EPR) calculation curve generated from DSAS for riverbank line change (m/year) of the Vistula River (#17) in the middle section between the mouth of the Radomka River (km 430) and of the Narew River (km 551): A – left bank, B – right bank. X-axis shows the transect number. The numbering of the transects increases from south to north.



V. Area-based approach for rivers. The area-based method was used to assess river planform changes was used similar to
295 the SCREAM method (Rowland et al., 2016) and REAL dataset (Langhorst and Pavelsky, 2023). Channel erosion was
measured as a bank retreat along the studied rivers based on the Global Surface Water Explorer (GSWE hereinafter) automatic
image interpretation dataset, which provides global data on the location and persistence of surface water and its changes from
1984 to 2021. Each year 14–22 space images (raster layers) that characterize periods of different water flow. In our research,
the “Water Transitions” layer was used, which provides an estimate of long-term water history by identifying transitions
300 between permanent water, seasonal water and land classes between the first and last years. Water surface area changes on the
images are mainly caused by water balance fluctuations; however, in the regional context of river channels, channel erosion
can be described as a new permanent water body adjacent to the modern river channel.

Another GSWE layer, “Occurrence Change Intensity”, provides information on where the surface water occurrence increased,
decreased or remained the same for 1984–1999 and 2000–2021, whereas the “Transitions” layer divides these changes into
305 eight classes based on seasonality and stability. Both classifications were compatible and were used similarly (Fig. 5). To
obtain the migration rate [m/yr] for each reach expressed, the right- and left-bank migration polygons were divided by the total
surface, then by the length of the oldest of the two channel banks and then by the number of years of the analyzed time interval.

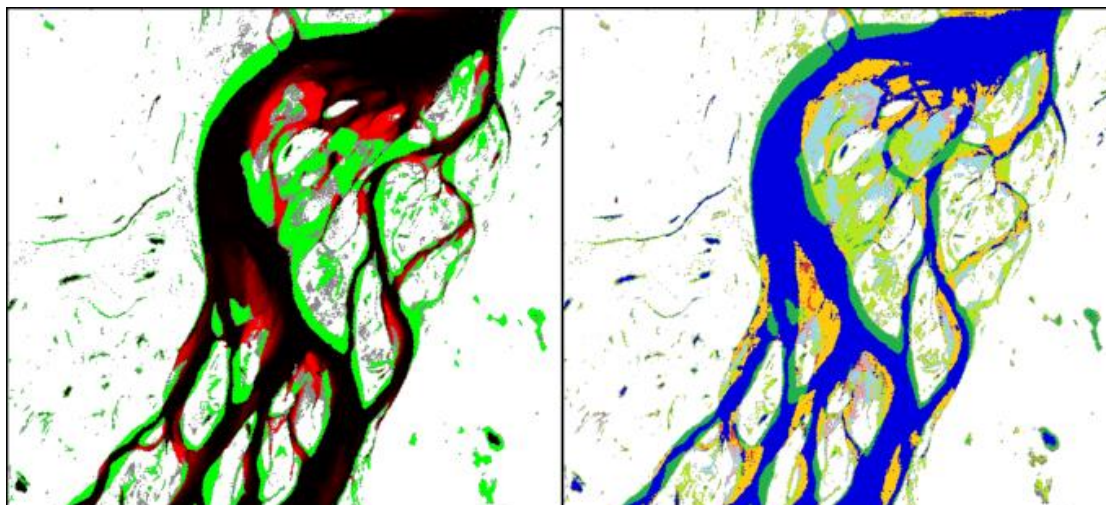


Fig. 5. Bank erosion classification according to GSWE map – change intensity (left) and transitions (right) (Lena River case study)

310 Also, manual area-based approach for distributary channels was conducted by comparing two Landsat satellite images with
similar water flow conditions for deltas of the Yenisey, Lena and Kolyma Rivers and long meandering stretches of Indigirka,
Oka, Chulyum, Ussuri and Yana rivers in homogeneous landscape and flow conditions. Bank locations were identified using
the AWEI water index, which made it possible to clearly distinguish the boundary between water and land and highlight hidden
details that are poorly visible when using only visible channels, including submerged shallows and shadowed sections (Feyisa
315 et al., 2014).



2.3. Compatibility of different methods applications and uncertainty estimate

The construction of the dataset involved a combination of manual and semi-automatic methods for estimating bank erosion, incorporating both field-based and remote-sensing data; consequently, multiple sources of uncertainty could affect the results. The dataset primarily showcases the potential of employing various methods to measure channel displacement rates and qualitatively comparing them across territories with diverse natural conditions and spatial factors driving erosion. Considering the scale of the observed phenomena, it's worthwhile to examine the extent of bank retreat extremes. In studies of bank erosion, the maximum values of bank retreat often receive the most attention, however, during the process of automatically defining a bank's edge, an increase in retreat distance typically results in a corresponding increase in error values or the likelihood of bank position error. Consequently, the results of automatic delineation necessitate thorough verification in this analysis due to disparities in bank failure patterns and the bank slope's configuration and incline.

Manual digitizing of high-resolution satellite or aerial imagery is the most accurate technique for bank retreat calculations, yet it is also the most labor-intensive due to a time-consuming process and limited accessibility compared to Landsat and Sentinel databases (Piégay et al., 2020). The availability of archived satellite and aerial imagery enables a substantial expansion of the comparison. The accuracy of manual delineation is influenced by the reference scale used during the process, which is often referred to as the "eye altitude," and typically remains below 1-2 meters of error. The primary causes of manual digitization mistakes are tied to the precision of georeferencing (both the primary and secondary images) and variations in tilt angle. A case study of the Mekong Delta (Binh et al., 2020) found that the total digitization error was no more than 2.8 metres.m. Up to this point, numerous methods have been devised for categorizing optical images and determining landscape boundaries from them, resulting in comparable levels of accuracy to manual digitization, specifically 0.4 to 12.7% for the erosion area in the Colville River case study (Payne et al., 2018).

The accuracy of our riverbank migration estimates was assessed by determining the bank erosion rate for several river stretches using multiple approaches. The middle course (#1) of the Lena River included several reaches that were observed on islands and on both the right and left banks, as shown in Table 3. Images captured by Landsat 5 in August 1999 and Landsat 7 in August 2020, both taken when water levels were low, were manually digitized to verify the GSWE results for the corresponding timeframe. The error was determined by comparing it to the percentage discrepancy between manual tracing and erosion detection. The findings suggest a compatibility range of 0.4 to 4.1%, thereby supporting the idea of compatibility among the tools used in this study.

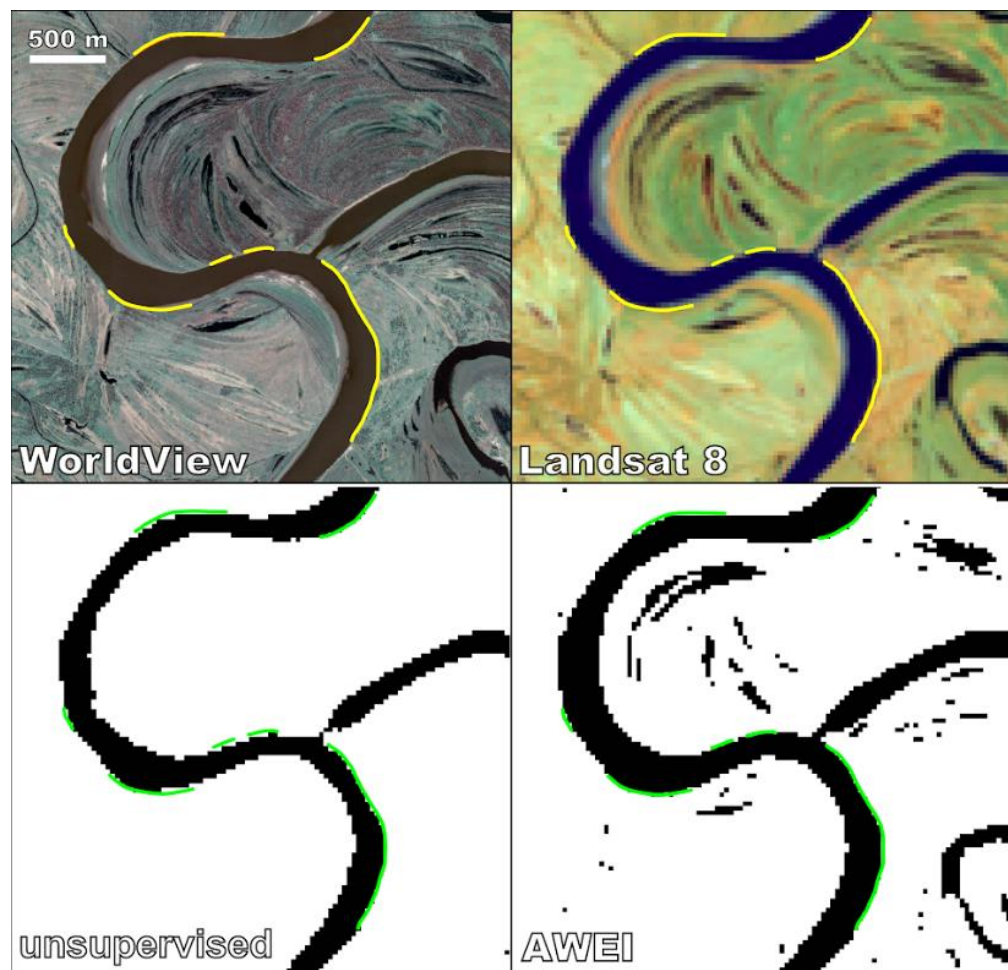
Table 3. Validation of area-based calculations

Reach length, km	Areas of bank erosion A, m ²		Error, %
	Manual digitizing	GSWE	
5	1,646,531	1,612,004	2.1
4	1,038,047	999,325	3.7



3	354,990	353,679	0.4
3	652,891	648,843	0.6
8	2,396,625	2,297,342	4.1

345 Previous studies (Albertini et al., 2022; Huang et al., 2018; Laonamsai et al., 2023; Liu et al., 2022; Zhou et al., 2017) have
evaluated the precision of different water surface definition indices in identifying the precise location of riverbanks, with
results showing that indices like MNDWI and AWEI yield an average error rate of up to 5%. The results indicated that
automatic computations can be applied when the rate of streamflow surpasses 100 m³/s, thus enabling the calculation of
outcomes with an accuracy of under 10%. The accuracy of optical extraction is constrained by various morphological features
350 of the banks, such as sandbars and debris resulting from bank material collapse near the edge, the shadows cast by the banks
and trees, and fallen tree trunks. A similar investigation was carried out for the portion of the Yana River that was examined,
employing multispectral (Landsat 8) and optical (WorldView-2) images acquired on 21/06/2021, as shown in Figure 6. Banks
were automatically classified using unsupervised classification and the AWEI index in Landsat imagery. For the comparison,
the images were also digitized at a scale of 1:500 using a high-resolution photograph. The research shows that automated
355 methods for marking bank positions result in minimal average errors when dealing with uniformly well-lit slopes and the
water-dry land boundary, but the error rate increases for other conditions. At the same time, the average error for the 6 assessed
locations (after smoothing the bank line using the Savitzky-Golay method) was 7.5 meters for automatic classification and 3
meters for the AWEI index. Annual retreat rates combined with prolonged periods of comparison will lead to extremely low
total percentages, specifically less than one percent.



360

Fig. 6. Yana River section on satellite images from June 21, 2021 with digitized position of the riverbanks in the erosion area (top) and an example of their automatic detection by automatic classification (bottom left) and with application of the AWEI index (bottom right).

Uncertainty can also be attributed to fluctuations in river water levels. To minimize this source of error, discharge estimates for all rivers were utilised for the image dates in question, ensuring conditions with a discrepancy of less than 5%. The greatest inaccuracies are typically seen when employing the centerline migration approach, primarily due to variations in flow rate. The placement of centerlines is influenced not only by the local characteristics of the erosion site but also by the entire width of the channel, making low-water images unsuitable for this approach, and it is essential to select an image taken on a date with discharges similar to those at bankfull conditions. The error was estimated by comparing the results of manual digitization for different sections of the Irtysh River, using pairs of images taken on different dates, with one pair corresponding to the same stage of the water regime and another pair to similar discharge levels. The analysis revealed discrepancies of up to 7.4% in average annual retreat rates and up to 6.3% in maximum rates when comparing yearly rates calculated from different image pairs (Table 3).

370



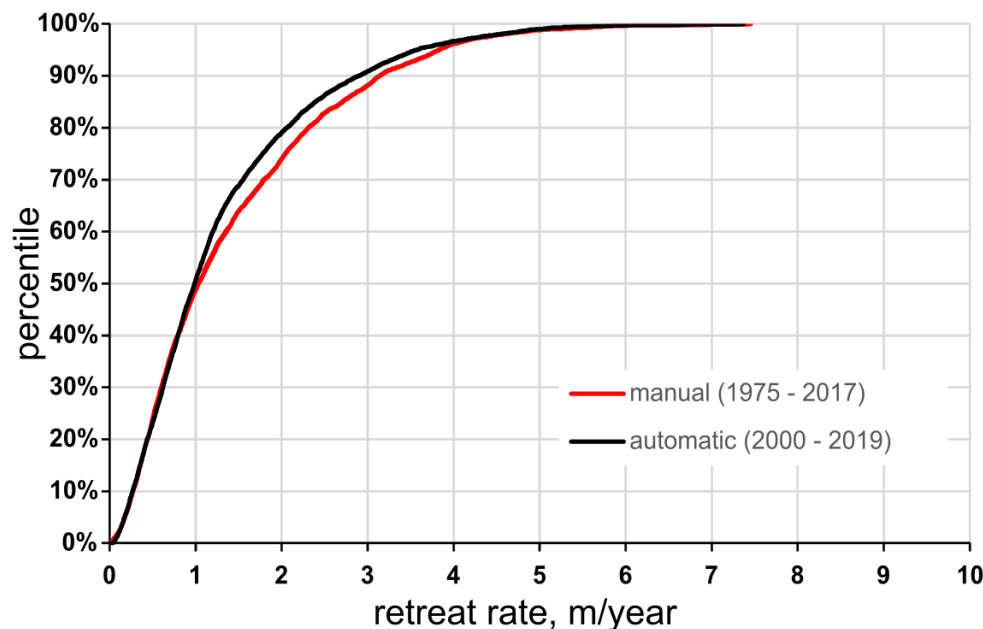
Table 3. Validation of erosion-rate-based calculations

Bank erosion rates, m/year (mean/max)		Error, % (mean/max)
Same phase of the water regime (Aug 1987 – Aug 2020)	Similar water flow conditions (13/09/1987, 2040 m ³ s ⁻¹ – 25/09/2020, 1990 m ³ s ⁻¹)	
7.6 / 12.6	8.0 / 12.2	5.3 / 3.3
6.8 / 12	7.3 / 12.8	7.4 / 6.6
10.9 / 16.4	11.4 / 17.2	4.6 / 4.9
9.5 / 15.6	9.7 / 15.6	2.1 / -
9.0 / 14.4	9.2 / 15.3	2.2 / 6.3
5.9 / 9.6	5.8 / 9.6	1.7 / -

375

We compared retreat rates from key river sections using both semi-automatic and manual methods across various time periods to evaluate the hypothesis that retreat characteristics become more consistent with longer comparison intervals. The data collected at the key sites on the rivers within the Ob basin (#10) were found to be similar when obtained using both semi-automatic and manual methods, and allowed for results with an acceptable error margin of up to 10%. Statistical analysis of the 260-kilometer Indigirka river section, which was digitized both manually (using high-resolution images from KeyHole and WorldView over a 42-year period from 1975 to 2017) and semi-automatically (using Landsat imagery over a 19-year period from 2000 to 2019), revealed that at cross-sections with a 30-meter frequency, the error in the mean retreat rate is approximately zero for half of the sections with either small or extreme retreat rates, even when comparing different periods (as shown in Figure 7). Automated retreat rates for the longer time period are overestimated by approximately 6.5% compared to manually calculated ones. Based on the above comparisons, we conclude that the retreat rates, aggregated in the presented database, are comparable to each other despite using different spatial approaches and time scales, and the total error of the obtained rates does not exceed 10%.

385



390 **Fig. 7. Percentile curves of the retreat rates for manual and semi-automatic delineation of banks on the similar section of the Indigirka River.**

DSAS approach (methods IV) was verified by comparing measurements from three control cross-sections using geodetic measurements with a GNSS RTK receiver for the Wistula River. The 2006 data came from measurement cross-sections provided by State Water Holding Polish—Water Management Authority in Poland. The validation results show that DSAS signifies its utility and reliability—the correlation coefficients ranged from 0.95 to 0.99. For example, study by (de Lima et al., 2021), the in-built EPR4Q for QGIS was validated with DSAS, depicting a high correlation coefficient range of 0.98 - 1.00 across various types of shorelines, thereby affirming the accuracy of DSAS in shoreline change assessment. (Gómez-Pazo et al., 2021), the ODSAS ("Open Digital Shoreline Analysis System"), was developed and it was compared with the DSAS, which yielded similar results. These studies highlight the credibility of DSAS in bankline and shoreline assessments.

2.4. Sediment yield estimates

400 Volume assessments of bank erosion used in the paper using formula (1), which involves determining the eroded area through manual satellite data processing or automatic image classification data from GSWE.

$$W_{ch} = \frac{S_{er} \cdot \rho_{sed} \cdot (h_b + h_d)}{\Delta t}, \quad (1)$$

With ρ_{sed} – riverbank sediments density [kg/m^3], Δt – time gap between satellite images (y), S_{er} – eroded area from satellite data [m^2]; h_b – bank height [m]; h_d – river depth [m].

405 The bank height (above average iced low-flow period water level h_b) was obtained from Arctic DEM digital elevation model with a resolution of 2 m (Morin et al., 2016). The bank height calculation was made using programming in the R language (*terra* and *sf* packages). For each group of adjusted pixels of channel erosion area S_{er} , a buffer zone of 50 meters radius was



created from which the maximum and mean value of absolute height was calculated using Arctic DEM data. To exclude the influence of canopy, buildings and other outlier errors, values of 0.95 and 0.05 quantiles was used. The difference between
410 maximum (0.95 Q) and minimum (0.05 Q) value of elevation of each buffer zone can be described as the difference of the low-flow period level of the river and the present bank and floodplain height.

The underwater part of bank slope was obtained as a mean depth of river using the 1D Shezi formula (2–4) based on data obtained from global datasets HYDROAtlas (Linke et al., 2019) and GRWL (Allen and Pavelsky, 2018) under average annual flow conditions. Data of mean annual discharge and water slope were obtained from HYDROAtlas with mean resolution of
415 ~4 km. Data of mean river width was obtained from GRWL with mean resolution ~3 km. The Manning's roughness coefficient is assumed as constant for all rivers as 0.045 (Baryshnikov, 1990).

$$Q = \omega \cdot C \cdot \sqrt{RI}, \quad (2)$$

$$C = \frac{1}{n} h^{\frac{1}{6}}, \quad (3)$$

$$h_d = \left(\frac{Q \cdot n}{B \cdot \sqrt{I}} \right)^{\frac{3}{5}}, \quad (4)$$

420 with Q – water discharge [$\text{m}^3 \text{sec}^{-1}$]; ω – cross-section square [m^2]; C – Shezi coefficient [$\text{m}^{0.5} \text{sec}^{-1}$]; R – hydraulic radius [m]; that is similar as river width B ; I – slope; n – roughness coefficient.

An evaluation of the bulk density of riverbank sediments was comprised as for typical rivers sediment values from (Karashev, 1977) and included into the dataset as additional parameterization (see 2.5). Also, the height of the eroded bank edges was obtained from the ArcticDEM elevation model. Bank edge height is calculated automatically using the Extreme Difference
425 Estimator method in the R environment that searches for graph inflections (corresponding to the seam and the edge of the coastal slope) and records the difference in the heights of the inflection points in each transect. The output is erosion sections, formalized into points located along their central line with the required density. Each point contains all the required information for further processing – erosion width, erosion wall height, and distance along the bank line.

2.5. River reach classifications

430 Additionally, each river section was characterized by natural drivers of channel evolution. The annual water discharge and river characteristics were taken from the HydroATLAS database (Linke et al., 2019) with a spatial resolution of 10 km. Attribution of river to natural zones was done based on the Köppen climate classification (Peel et al., 2007), which is indexed based on three letters of the classification scheme (e.g., BSk relates to a dry [B], semi-arid [S], cold [K] climate).

Permafrost zones were categorized based on actual area underlain by permafrost from Obu et al. (2019). Finally, rivers were
435 classified by channel patterns distribution according to the map: “Channel morphology regime of rivers of USSR” (Chalov et al., 2018) and further classified by dominant bed-deposit types. Each bed deposit class (from sand to gravel) was characterized by specific values of grain density (see Table 4), which is used to estimate volumes and masses of sediment delivery to river channels.

Table 4. River classifications used in the dataset



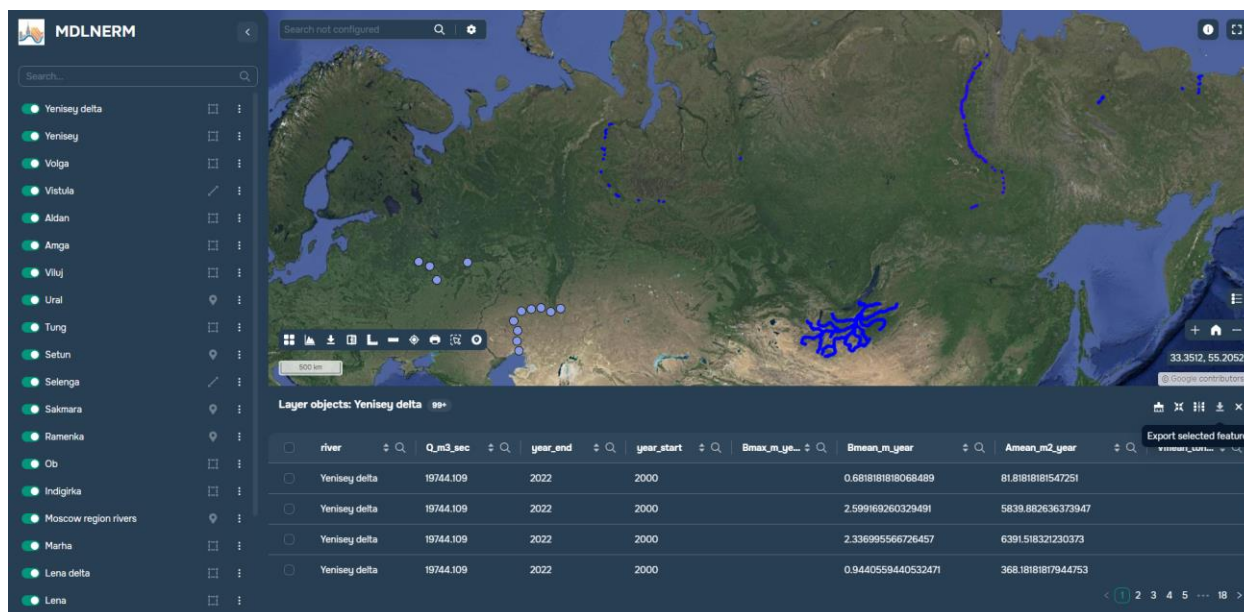
Parameter	Classes			Description	Source
Water runoff	(m ³ /s)			Unique values for each bank retreat site with 10 km averaging	HydroATLAS (Linke et al., 2019)
Permafrost	Cont			Continuous permafrost domain 90%>	(Obu et al., 2019)
	Discon			Discontinuous permafrost domain 50–90%	
	Spora			Sporadic permafrost domain 10–50%	
	Isol			Isolated permafrost domain 0–10%	
Natural zone	A Tropical	f Rainforest		The Köppen climate classification	(Peel et al., 2007)
		m Monsoon			
	w Savanna, dry winter				
	s Savanna, dry summer				
	B Dry	W Arid desert	h Hot		
	S Semi-arid steppe	k Cold			
C Temperate	w Dry winter	a Hot summer			
	f No dry season	b Warm summer			
	s Dry summer	c Cold summer			
D Continental	w Dry winter	a Hot summer			
	f No dry season	b Warm summer			
	s Dry summer	c Cold summer			
		d Very cold winter			
E Polar	T Tundra				
	F Ice cap				
Geology	209 kg/m ³ – Yedoma outcrop			Mean value of sediment density with an ice content assessment by (Kizyakov et al.,	Map: “Channel morphology regime of rivers of USSR”



		2024) (Fuchs et al., 2020)	
	1,100 kg/m ³ – Sand with silt river sediments 1,500 kg/m ³ – Sandy sediments 1,700 kg/m ³ – Sand with gravel sediments 2,100 – Gravel boulder sediments	Sediment density based on mean sediment diameter by (Karaushev, 1977)	

440 **2.6. Online platform**

The multi-tool dataset on Large Northern Eurasian Riverbank migration (NERM) is realized via platform GISCARTA, which provides online access to the dataset, its visualization, and download of data as GEOJSON and text files of attributive tables (Fig. 8). All features of the database, polygons of bank retreat, points of maximum values of bank erosion centrelines, have their attribute parameters each in a separate column. There are values of bank retreat rates in meters per year (Bmean), channel erosion area in square meters per year (Amean), mass of channel erosion in tons per year (Vmean), maximum values of bank retreat (Bmax), start and end years of satellite images (year_start, year_end), name of the river (river), mean annual water discharge (m³/sec). The platform is available via the link (<https://map.giscarta.com/viewer/93a6a4b3-179f-450f-be02-a31ca6db245b>). The dataset is constantly updated and includes broader results than those discussed in the paper. In addition, it is possible to get access to the data in Zenodo, where ESRI shape files are stored (Chalov, S., Ivanov, V., Danila, S., Pavlyukevich, E., Habel, M., Botavin, D., Chalova, A., Golovlev, P., Kamyshev, A., Kolesnikov, R., Koneva, U., Kurakova, A., Mikhailova, N., Tuzova, E., Prokopeva, K., Zavadsky, A., Acharyya, R., Chalov, R., Varenov, A., 2024). Using large datasets and considering evolutionary trends, aggregating data via boxplots provided an effective method for synthesizing results and addressing key discussion points.



455

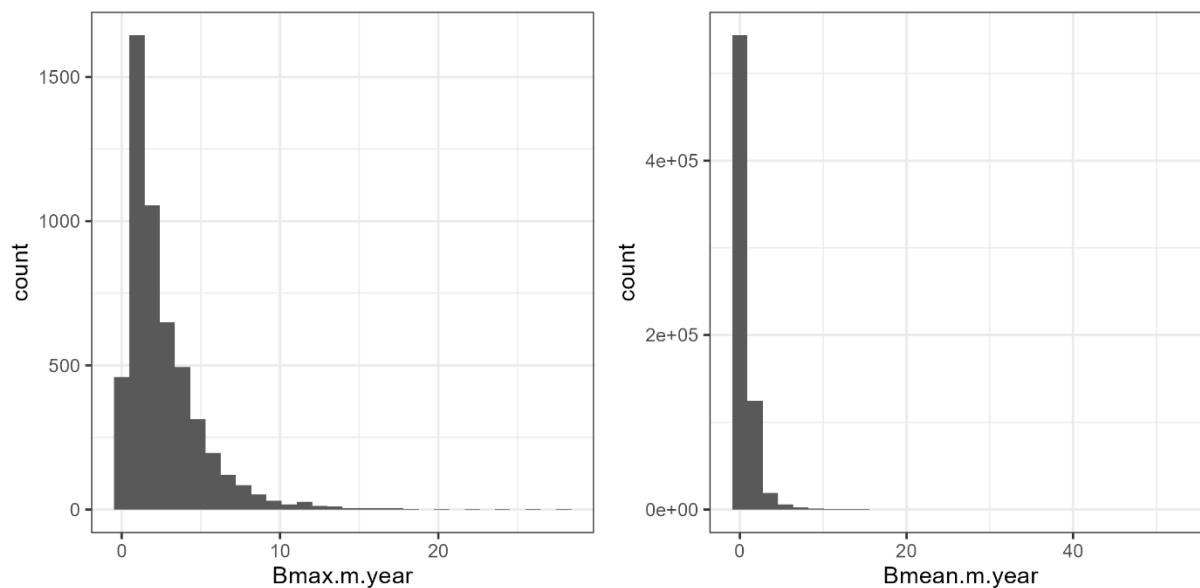
Fig. 8. GISCARTA platform screenshot

3 Results

In total, this dataset consists of a multi-tool dataset of channel erosion rates for 257 rivers and three deltas with annual mean water runoff data from less than $0.2 \text{ m}^3/\text{s}$ in small rivers of Moscow city region to $19,700 \text{ m}^3/\text{s}$ in the Yenisey downstream. It covers 626 772 reaches with defined bank retreat rates for the 20–30 years and more. The spatial resolution of the reaches in the dataset is from 10 m to 2 km.

Values of mean bank erosion rates for whole rivers ranges from 0.01 to 53 m/year. Only for the manual data from Kudma catchment (18) is there no calculation of this parameter. Mean value of this series is 1.38 m/year, median values is 0.83 m/year. The quartile of 75% has the value of 1.62 m/year, and for the 25% quartile this value is 0.54 m/year. The distribution of the observed riverbank migration rate is approximately gamma (Fig. 9).

Much smaller rivers contain parameters of maximum bank retreat (m/year) that can be detected through methods I and II. Within 21 rivers processed by these approach ($n = 2859$), values of maximum bank retreat for whole rivers are between 0.01 and 26.3 m/year with a mean value of 2.53 m/year. The quartile of 75% has a value of 3.39 m/year, and its 25% is 0.88 m/year. The distribution is log-normal.

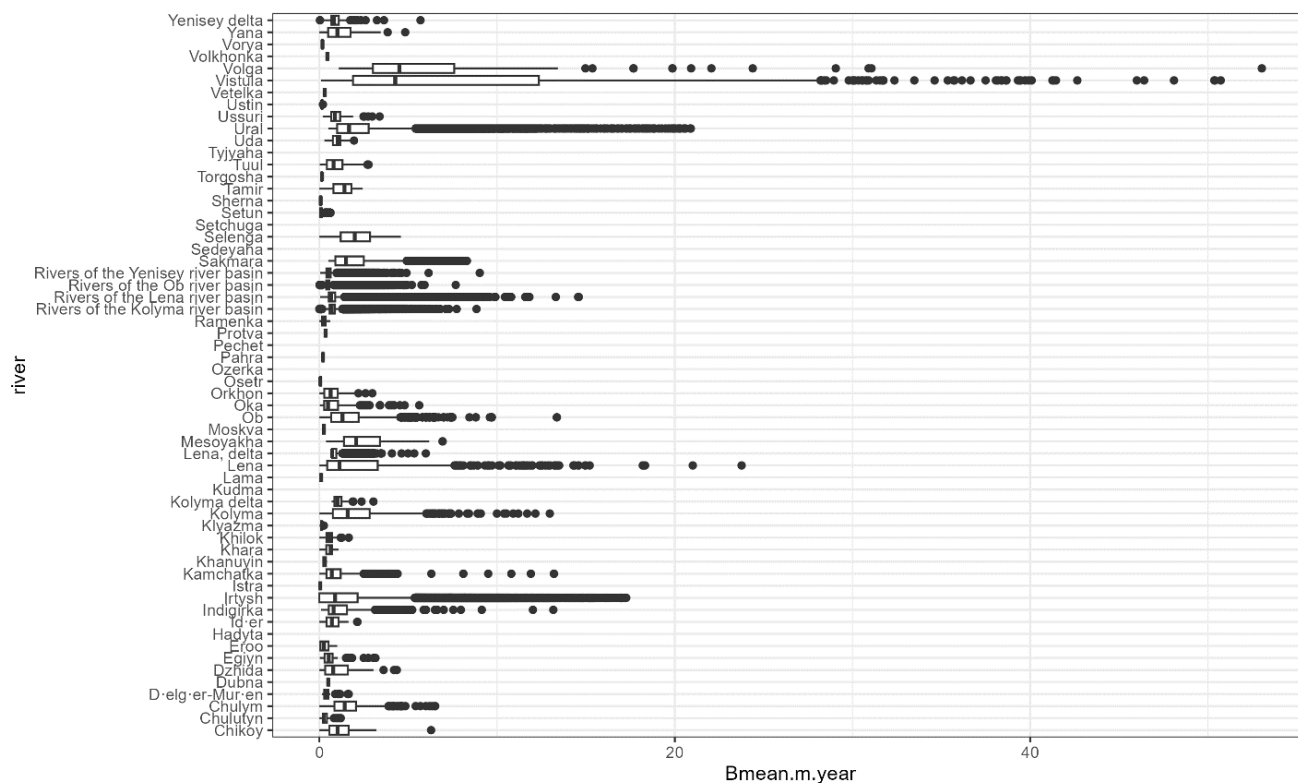


470

Fig. 9. Distribution of observed riverbank erosion rates in Northern Eurasia (left – annual bank retreat B [m/year]; right – maximal bank retreat B [m/year])

To describe this dataset, the boxplot method was used to describe Bmean, Bmax and Amean (Fig. 10, 12, 15). Boxplot content here are “minimum” value (Q1 - IQR), first quartile [Q1], median – line, mean – cross, third quartile [Q3] and “maximum”, (Q1 + IQR), outliers – point) – of sediment flux rate (Mt/year/km). IQR is the interquartile range (IQR) or the 50 percent of data points lying above the first quartile and below the third quartile. The largest values of mean bank erosion are for the Vistula and Volga Rivers (Fig. 10).

475



480 **Fig. 10. Distribution of mean annual bank retreat values by rivers**

The largest values of maximum bank retreat are for the Ob, Kamchatka and Indigirka Rivers. Values of eroded areas due to bank retreat (A_{mean}) for whole rivers banks are in the ratio between 0.01 and 226,000 $m^2/year$. This parameter was estimated for 15 rivers that were processed by methods II, III and V. The mean value of this maximum bank retreat is 913 $m^2/year$; the median values is 46 $m^2/year$. The quartile of 75% has a value of 130 $m^2/year$, and its 25% is 28 $m^2/year$.

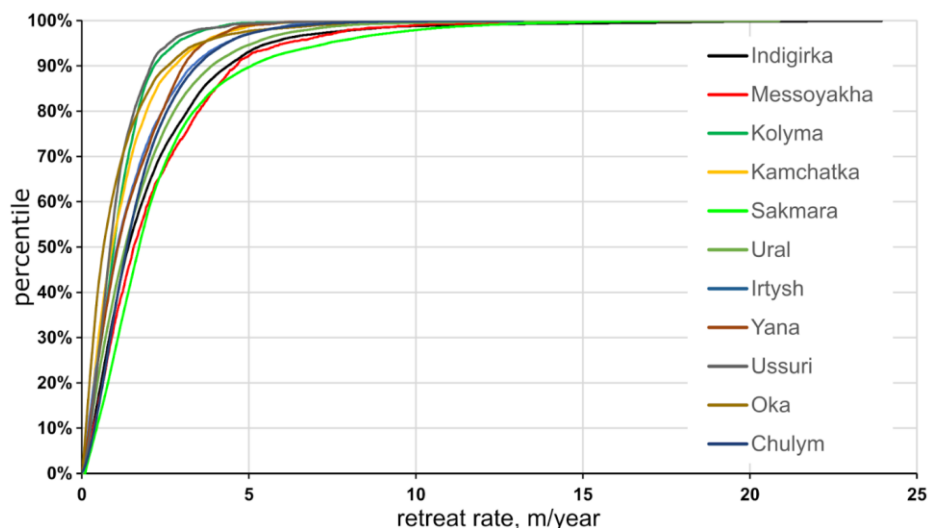
485 Values of mean annual bank erosion volumes (V_{mean}) for the banks of whole rivers are in the range between 0.01 and $11 \cdot 10^6$ ton/year. This parameter was esteemed only for eight rivers that were processed by method III. The mean value of V_{mean} is 17,000 ton/year; the median value is 889 t/year. The quartile of 75% has a value of 2,500 ton/year, and its 25% is 407 ton/year. The largest values of maximum bank retreat are for the Lena and Kolyma Rivers.

Significant total length of the analyzed sections allows retreat rates to be assessed in a statistical way by estimating the recurrence of different scour rates along the length of the eroded sections. Their total length for the studied rivers ranges from 24 to 49% of the total length of the banks, reaching maximum values at sections with completely unrestricted meandering. Resulting percentile curves shows the comparative rarity of extreme bank retreat rates (Chalov and Shkolnyi, 2018), which, at the same time, determine the main portion of eroded areas and sediment source in the considered rivers (figure 11).

The combined length of the sections studied allows for the assessment of retreat rates through statistical analysis, which entails determining the frequencies of different retreat rates along the eroded sections. Their total length for the studied rivers



comprises between 24 and 49% of their total length along their banks, with the highest percentages being found in sections with completely unrestricted meandering. The resulting percentile curves demonstrate the comparative scarcity of extreme bank retreat rates (Chalov and Shkolnyi, 2018), which, concurrently, account for the majority of eroded areas and sediment sources in the studied rivers (figure 11).



500

Figure 11. Percentile curves of the retreat rates for the observed rivers' eroding sections

4. Discussion

4.1. Drivers of riverbank migration across Northern Eurasia

The presented dataset is different from previous products in that it contains information on small, medium and large rivers alike. By attributing mean bank retreat rates to annual discharges (Fig. 12), our results confirms that size is the first-order control on riverbank erosion at large scales following previous estimates of large rivers (Langhorst and Pavelsky, 2023). The general relationship of B_{mean} and annual discharge Q is explained by quadratic law: $B_{mean}=f(Q^2)$. At the time influence of river size control is rather as far as riverbank erosion is complex, with many different processes and mechanisms depending on multiple forcing parameters working in tandem and varying both spatially and temporally. Among them, channel patterns and stream geometry, bank composition, water temperature and soil moisture, which all impact both separately and jointly to bank erosion rates, and related to also climatic, geological and other drivers.

510

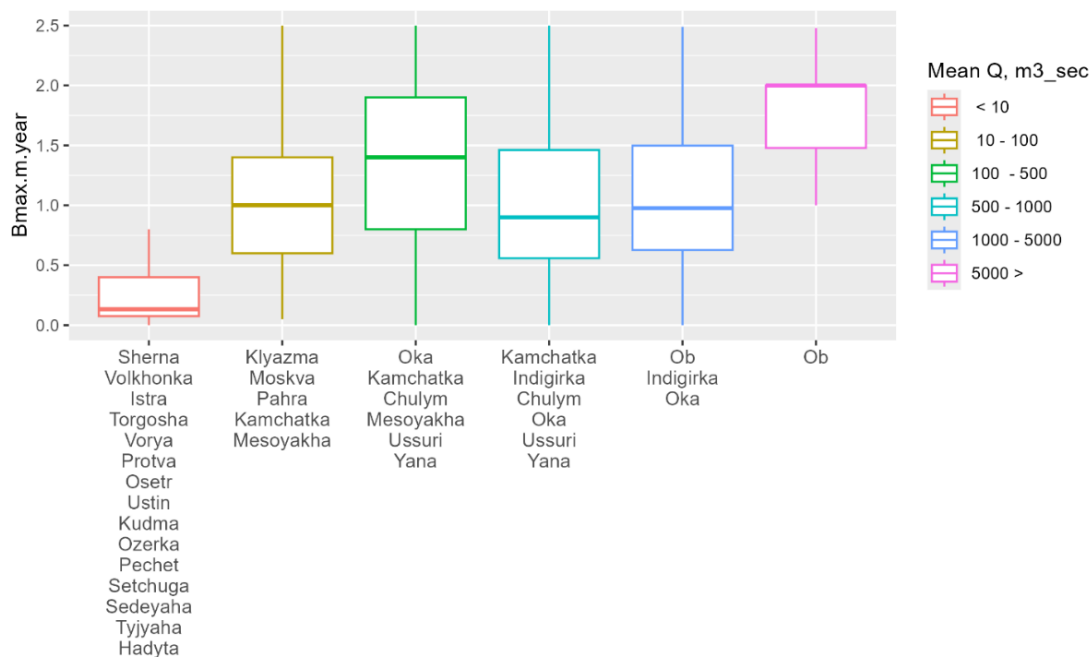


Fig. 12. Boxplot of reach-averaged bank retreat rates with respect to river size (annual discharge Q [m^3/s])

The first order capturing these drivers' influence is specific to each catchment or river. The NERM dataset provides sufficient information to assess the impact of catchment and longitudinal changes on bank-erosion mechanisms. Such an example is provided by the bank migration of the Ob River, which is the longest river in Northern Eurasia, with an average B_{mean} of 2 $\text{m}/\text{year}^{-1}$ (Fig. 13a). The mean annual erosion rate of banks in the upstream Ob is 2.4 $\text{m}/\text{year}^{-1}$, while the maximum annual erosion rate is 26.3 $\text{m}/\text{year}^{-1}$. In the sections of the Ob River located downstream from the Novosibirsk reservoir, erosion rates decrease (mean annual erosion rate is 1 $\text{m}/\text{year}^{-1}$, maximum annual erosion rate is 6.6 $\text{m}/\text{year}^{-1}$). The latitudinal section of the Ob River (from the confluence of the Ob River and the Vakh River to the confluence of the Ob River and the Irtysh River) shows an increase in average rates of bank migration to 2.5 $\text{m}/\text{year}^{-1}$, and a maximum rate of erosion of 16.4 $\text{m}/\text{year}^{-1}$. Downstream Ob shows similar riverbank migration rates as at the latitudinal section of the Ob River (mean annual erosion rate is 2 $\text{m}/\text{year}^{-1}$, maximum annual erosion rate is 17 $\text{m}/\text{year}^{-1}$). The area of erosion on the Ob River has increased from almost 4 million square meters in the sections located downstream from the Novosibirsk reservoir to over 120 million square meters on the downstream Ob (Fig. 13b).

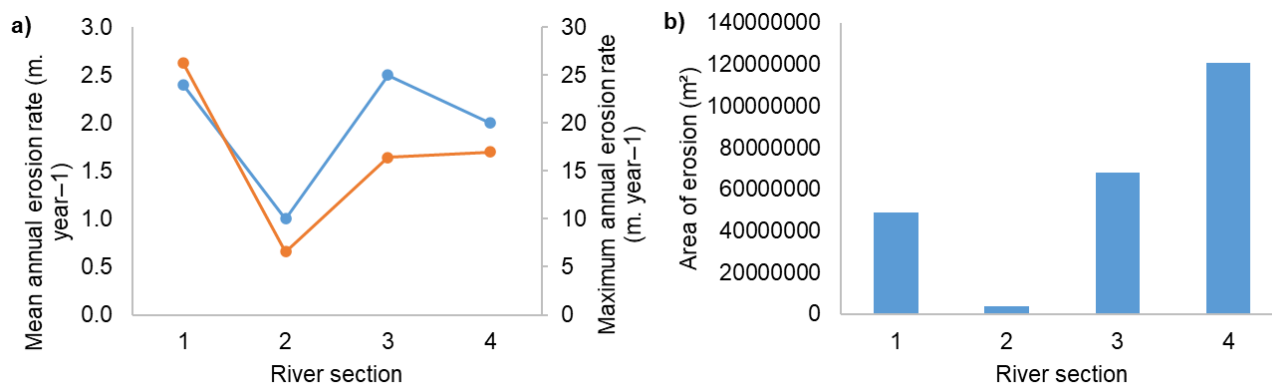


Fig. 13. Riverbank erosion of the Ob River: a – erosion rate, b – area of erosion. 1 – Upstream Ob River, 2 – Middle stream of Ob River (from the Novosibirsk reservoir to the confluence of the Ob River and the Tom River), 3 – Middle stream Ob River (from the confluence of the Ob River and the Vakh River to the confluence of the Ob River and the Irtysh River), 4 – Downstream Ob River (from the confluence of the Ob River and the Irtysh River to the city of Salekhard)

530

535

540

545

The mean rates of bank retreat are modeled using a gamma distribution due to the presence of extreme rates of riverbank migration. Extreme bank erosion on large Northern Eurasia rivers is frequently more rapid than average rates due to certain factors, such as low-density material like pyroclastic sand found on the Kamchatka River (Chalov et al., 2021) or permafrost layers as reported by (Gautier et al., 2021). The greatest rates of platform change are typically found on large rivers featuring complex braided channels. The spatial analysis of erosion rates along rivers reveals extreme bank retreat rates that significantly exceed the 95th percentile. On average, the river's retreat is typically around 2% of its width annually, with a yearly rate of between 2 and 15 meters for the larger rivers in the study. In the area surrounding the Partizan settlement, near the Lena River, extreme values of long-term measurements reach 35 meters per year. This is particularly evident where discharge from various branches converges into a single channel, causing a significant bend with a curvature ratio of approximately 2. The Indigirka River at Sypnoy Yar exhibits annual retreat rates of up to 24 meters; in this location, the receding right bank of the river is a 30-meter high plateau ledge formed from frozen sands. In the two described regions, erosion results in the delivery of several million tons of sediment annually, which in turn leads to the formation of riffles downstream and poses challenges for navigation. The rate of bank erosion on the Kamchatka River is not as extreme as some others, with a maximum annual retreat of up to 7 meters, but it can still cause the river width to decrease by 10% or more each year, resulting in the quick movement and cyclical meanders cutoff.

550

The NERM dataset provides information on other drivers at the scale of Northern Eurasia – e.g., it also shows the importance of climatic impacts which can be seen at graphs dividing retreat rates on climate zones by Koppen classification and latitudes (Fig. 14). Mean annual bank retreat rates are decreasing from south to north (from 1.9 ± 0.8 m/year within the 40–50° zone to 0.5 ± 0.2 m/year within the 70–75° zone).

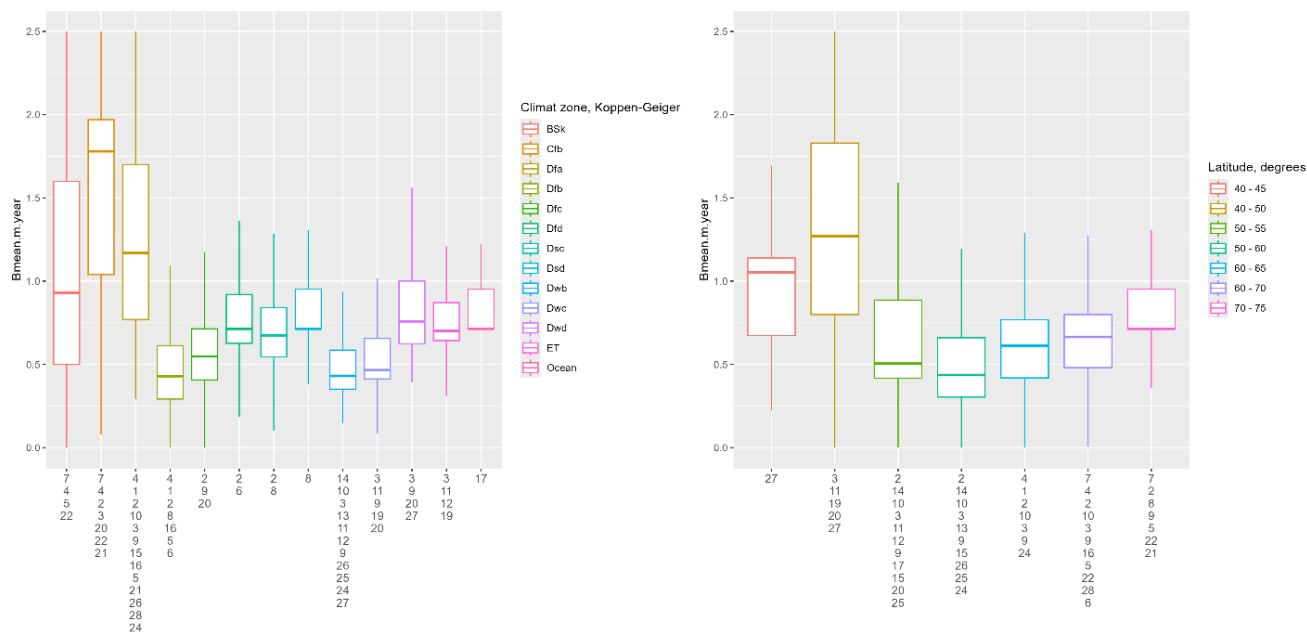
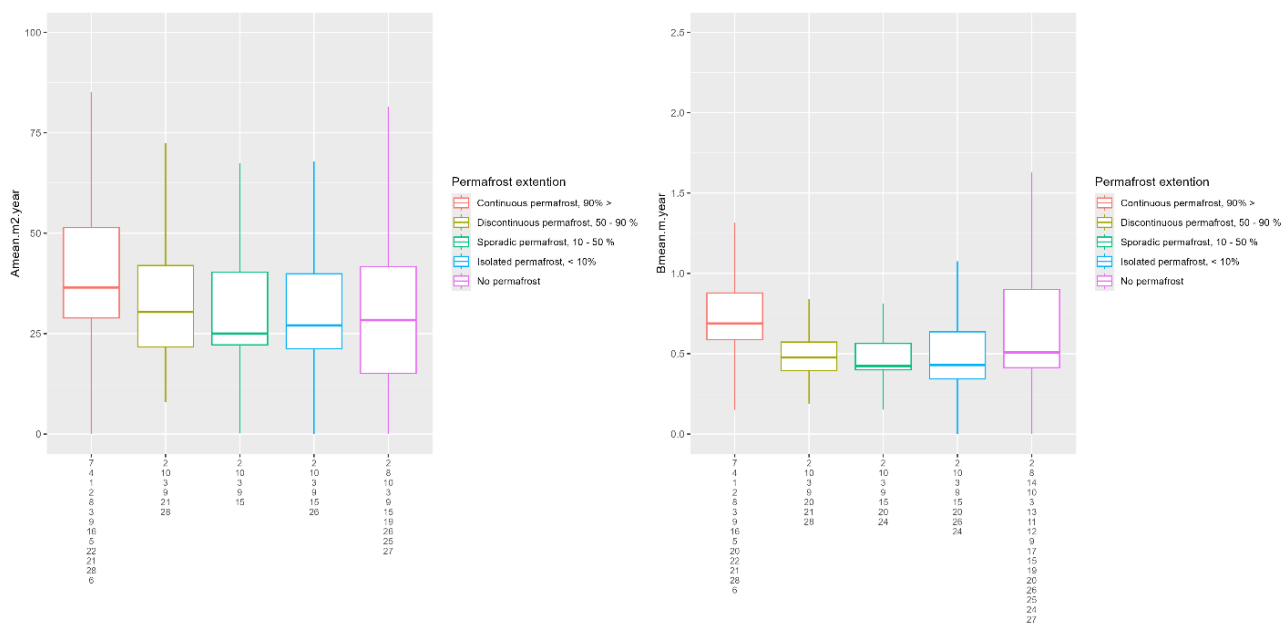


Fig. 14. Boxplot of reach-averaged bank retreat rates with respect to climate zones by Koppen classification (see explanations in the text) and latitude

555 Another natural driver that plays an important role in the channel evolution of Northern Eurasia rivers is permafrost (Rowland et al., 2010). The distribution of bank erosion rates in different permafrost zones reflects contrasting impacts of permafrost on riverbank migration. The average rate of bank retreat (B_{mean} [m/year]) varies in NERM from 1.3 ± 0.8 m/year in the permafrost-free zone to nearly 1 m/year where permafrost exists. By contrast, the areas of riverbank retreat (A [$m^2/year$]) increase with the increase in permafrost distribution (Fig. 15). This enables to conclude that thermal erosion in combination

560 with mechanical erosion determines the greater susceptibility of riverbanks to destruction in the permafrost distribution zone, but the erosion rates of banks composed of permafrost soils are lower due to the soil adhesion mechanism. This thesis is generally in line with Rowland et al. (2023), who found for the past that erosion rates in permafrost-affected rivers were on average nine times lower than in non-permafrost-affected systems.



565 **Fig. 15. Boxplot of reach-averaged bank retreat rates with respect to permafrost (left – bank areas destroyed by bank erosion; right – average rates of bank erosion)**

These findings related to permafrost impact are confirmed at permafrost-affected rivers where data of channel changes was extended from 1950 to 1970 with the use of manual digitizing by Keyhole images. In the Lena River delta (#8), the highest bank migration rates are related to the ice complex (or Yedoma) areas. Specifically, up to 15% of the bankline may be eroded in the downstream of the Trofimovskaya and Olenekskaya branches (Fig. 16). The highest mean annual erosion rates occurred in yedoma on the Sobo-Sise Island with erosion area amounted to 0.58 km² over 21 years. The mean annual erosion rate is 4.74 m year⁻¹, and the maximum rate increases to 15 m year⁻¹. Due to a rise in air temperature rise from 0.86 °C per decade from 1979 to 2021 to 1.61 °C per decade during 2000–21 (Chalov et al., 2023a; Gelfan et al., 2017), there was an increase of 1.95 m year⁻¹ (or 95%) in 2000–21 compared to 1964–2000 (Fig. 16). The most significant increase in erosion rates (3 times between periods) is observed in the Olenekskaya branch and is also related with the ice complex on Kurungnakh Island. It is important to note that along ice-wedged complexes, the high rates of bank retreat remain stable (Sobo-Sise Island). Previous studies on channel migration for the Lena River Delta concentrate on the yedoma permafrost cliff on Sobo-Sise Island at Sardakhskaya branch (Fuchs et al., 2020). The cliff length is 1,660 m and the vertical heights are up to 30 m above mean river water level. The authors manually digitized the upper cliff line on the images from 1965 to 2018. Erosion rates vary from 4.8 to 15.7 m year⁻¹ in different parts of cliff, and the mean annual erosion rate is 6.1 m year⁻¹.

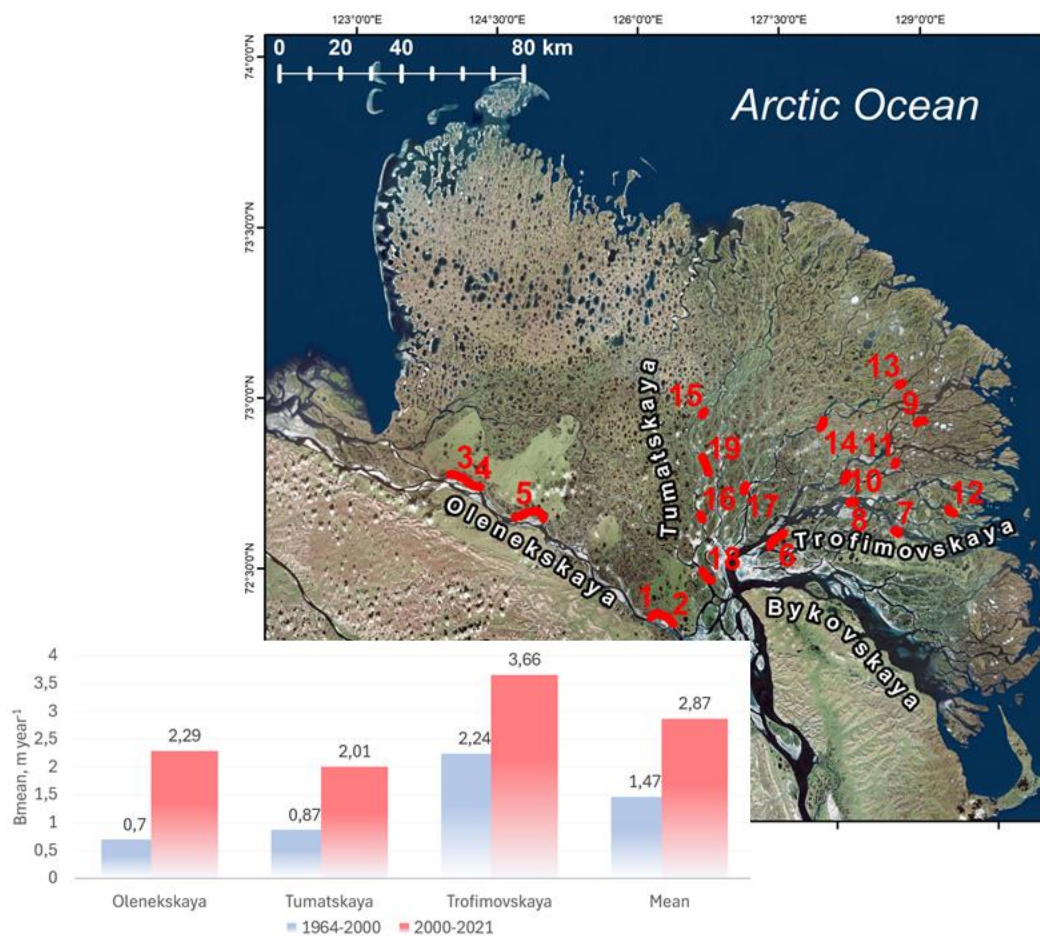
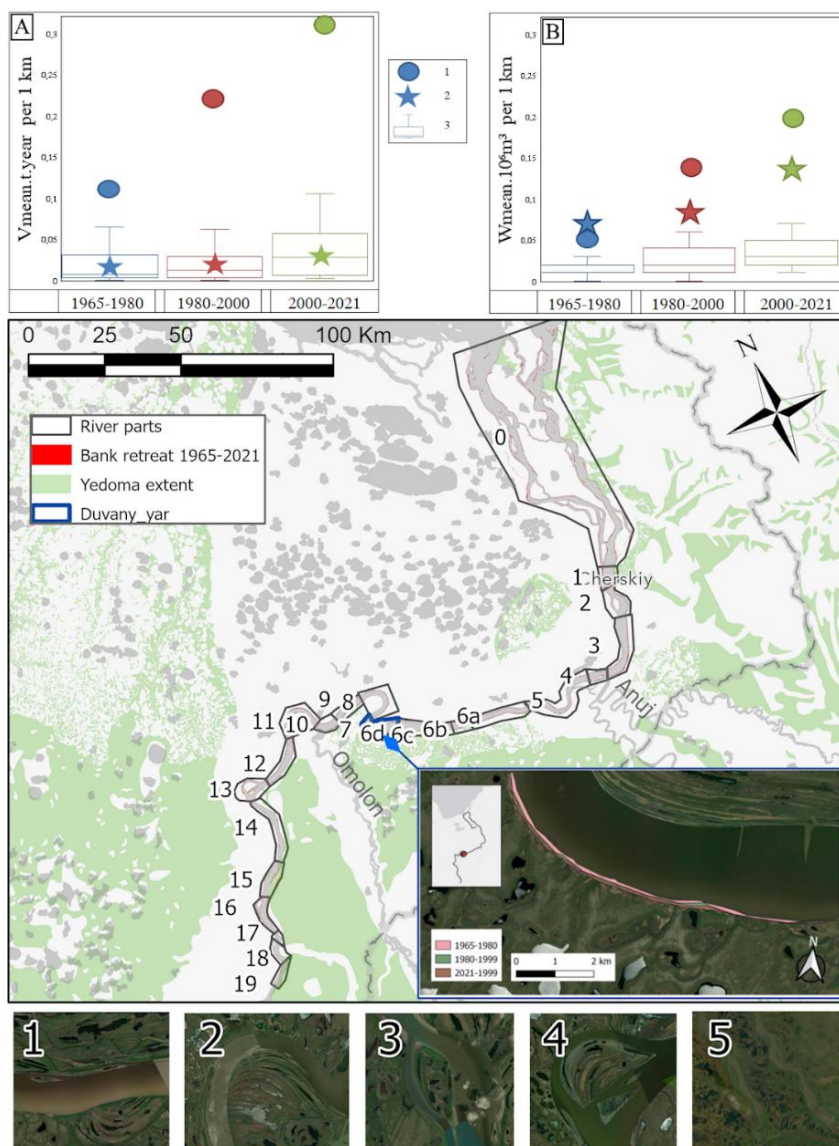


Fig. 16. Bank migration rates over Lena delta: location of riverine reaches with estimates (on the top, reaches are indicated by numbers) and values for different time spans (on the bottom) (© Esri Imagery)

585 Similar patterns are observed to those of the downstream Kolyma River, where a significant increase in riverbank migration rates was observed both upstream from the delta and within the delta. Similar climatic drivers here influence both the stability of ice-wedge complexes widely distributed along channel banks (Murton et al., 2015; Szumińska et al., 2023) and an increase in riverbank migration rates. It is interesting to note that the rates of channel migration were significantly higher within the delta during all considered periods (Fig. 17).



590

Fig. 17. Boxplot comparing the distribution of volume of bank retreat (left) and sediment mobilization due to bank retreat t/year (right) in 1965–80, 1981–2000 and 2000–21 in Kolyma upstream from delta (boxplots) and within delta (dots, reach 0 on the map). Stars indicate reach 6 on the map (Yedoma Duvanny Yar complex) (© Esri Imagery)

4.2. In-channel erosion contribution to sediment yield

595 The total volume of channel erosion is estimated at 151 million tons per year in the 1,680-km section of the lower Ob, 15.9 million tons per year in the 1,500-km section of the Yenisei, and 338 million tons per year in the 1,800-km section of the Lena. In the Selenga and the Kamchatka, the volume of channel deformations is comparable to the values typical for the lower course of the Yenisey River. On the Kamchatka River, the total eroded area during the comparison period (from 23 to 50 years, depending on the availability of satellite images for river sections) was 23.5 km², which corresponds to an average volume of



600 channel deformations of 670,000 m²/year. Thus for the Kamchatka, ~4.6 million tons of sediments per year enter the channel due to bank erosion. In some years, this value may increase because of the bends cutoff.

Sections of a braided channel exert the greatest influence on sediment runoff. In the Selenga basin, the maximum values of bank retreat (on average at the tops of bends from 9 to 16 m/year) are mainly situated in the section of the braided channel. At the same time, in the sections of the channel with wide floodplains, more than half of the entire area of bank erosion is related to the erosion of river islands. On the Lena River section from Pokrovsk to Zhigansk cities, 60% of the total volume of bank erosion is related to island erosion (11 thousand m² year⁻¹ km⁻¹), and it is 40% to erosion of the bedrock. The left and right banks have an equal ratio of 20% to each other (3.7-thousand m² year⁻¹ km⁻¹). The maximum intensity of bank erosion is associated with the incision of river valleys and sand bars. On all rivers, the ratio of the intensity of bank erosion of the right and left banks is approximately the same. For the left bank of the Kamchatka River, the length of the eroded banks is 37%, and for the right bank, it is 44%.

These combined results offer significant insights into the sediment budget of large river basins. In the lower reaches of the world's biggest rivers, the quantity of channel erosion debris that enters is roughly the same as the amount of sediment being washed away, and materials eroded from riverbanks are highly connected to the channel. Based on this, it can be inferred that the channel component of sediment runoff exhibits latitudinal zonality and is influenced by large-scale factors, which in turn are affected by river size. In the Ob River's middle and downstream sections (below where it meets the Vakh River), approximately 33.5 million tons of sediment enter the channel yearly due to channel deformations, which is lower than the sediment load at the river's mouth. The sediment influx into the channel due to bank erosion within the river basins of southern rivers, where unstable channels are common, often far surpasses the sediment discharge of rivers, as seen in the Selenga basin where it is 11-fold (Table 5). In the foothills, sediment runoff originating from rivers achieves high levels, with significant disparities in the extreme mitigation measures taken for channel control. In the Kamchatka River basin, the river itself carries two times more material eroded from its banks than is transported downstream in the sediment runoff, with at least half of this material accumulating in the riverbeds.

Table 5. Calculations of volume of material entering channels of the Selenga River and its tributaries as a result of bank erosion (within the main channel or main branch)

River	Total volume, m ³ /year	Total volume Ton/year*
Dzhida	847,198	1,440,200
Delger mörön	233,282	396,600
Ider	412,960	702,000
Orkhon	1,143,891	1,944,600
Selenga	7,304,712	12,418,000
Tamir	448,632	762,700



Tuul	684,115	1,163,000
Uda	454,782	773,100
Hanuyin	4,371	7,400
Hara	142,079	241,500
Khilok	509,027	865,300
Chikoy	1,577,407	2,681,600
Chuluut	67,734	115,100
Egiin Gol	396,272	673,700
Eroo	25,834	43,900
Totally from the catchment	14,252,297 m ³ /year	24,230,000 t/year
Accounting erosion of islands		26,700,000 t/year

625 5 Data availability

The presented datasets are available open access via the ZENODO repository (<https://doi.org/10.5281/zenodo.11072919>) (Chalov et al., 2025).

6 Conclusions

630 The NERM dataset offers the comprehensive riverbank migration assessment for particular areas. We utilised a unified dataset to examine statistical data on bank erosion, river discharge, and catchment factors, including permafrost extent and natural zone, using multiple analytical tools. River size was discovered to be a key factor in riverbank erosion. Confirmation of the role of secondary controls in Northern Eurasia has been established, encompassing permafrost distribution and diverse climatic/natural zones. NERM serves as a case study to refine and verify theoretical models, offering insights into sediment origins in river systems by integrating riverbank erosion rates with sediment mobilization from eroded riverbanks. The comprehensive dataset presented offers a potential insight that further research employing multi-statistical methods could reveal quantitative laws governing riverbank migration at regional or catchment scales, influenced by geological, hydrological, and climatic factors.

Author contributions.

640 SRC: Conceptualization, Investigation, Methodology, Supervision, Writing – original draft preparation, Writing – review & editing; VI: Conceptualization, Formal analysis, Methodology, Project administration, Investigation, Visualization, Writing –



original draft preparation, Writing – review & editing; DS: Investigation, Methodology, Writing – original draft preparation, Writing – review & editing; EP: Project administration, Writing – review & editing, Investigation; MH: Investigation, Writing – original draft preparation; AK: Investigation, Writing – original draft preparation; RSC: Investigation, Supervision; DB, AC, PG, AK, RK, UK, NM, ET, KP, AZ, RA, AV, LT, AT and DF: Investigation. All authors reviewed the manuscript.

645 **Competing interests.**

The authors declare that they have no conflict of interest.

Disclaimer.

The data are provided with no warranty.

Acknowledgements.

650 This work was supported by the grant of the The Government of the Russian Federation (Agreement [№075-15-2025-008](#) [date 27.02 2025](#)) and the state assignment of the Makkaveev laboratory of Soil Erosion and Fluvial Processes, Faculty of Geography, Lomonosov Moscow State University (CITIS 121051100166-4).

The authors used Paperpal AI Microsoft Word plugin and Trink AI Writing and Grammar Checker Tool for English grammar improvement.

655 **References**

Alabyan, A. and Chalov, R.: Types of river channel patterns and their natural controls, *Earth Surf. Process. Landforms*, 23, 467–474, 1998.

Albertini, C., Gioia, A., Iacobellis, V., and Manfreda, S.: Detection of Surface Water and Floods with Multispectral Satellites, *Remote Sens.*, 14, <https://doi.org/10.3390/rs14236005>, 2022.

660 Alexeevskii, N. I., Berkovich, K. M., and Chalov, R. S.: Erosion, sediment transportation and accumulation in rivers, *Int. J. Sediment Res.*, 23, [https://doi.org/10.1016/S1001-6279\(08\)60009-8](https://doi.org/10.1016/S1001-6279(08)60009-8), 2008.

Alexeevsky, N. I. ., Chalov, R. S. ., Berkovich, K. M. ., and Chalov, S. R. .: Channel changes in largest Russian rivers: Natural and anthropogenic effects, *Int. J. River Basin Manag.*, 11, 175–191, <https://doi.org/10.1080/15715124.2013.814660>, 2013.

665 Allen, G. and Pavelsky, T.: Global extent of rivers and streams, *Science* (80-.), 361, eaat0636, <https://doi.org/10.1126/science.aat0636>, 2018.

Babiński, Z., Habel, M., and Chalov, S.: Prediction of the vistula channel development between Wloclawek and Torun: Evaluation with regard to the new geological survey, *Quaest. Geogr.*, 33, 7–15, <https://doi.org/10.2478/quageo-2014-0025>,



- 2014.
- Baryshnikov, N. B.: Dynamics of channel flows and protection of natural waters, Leningrad, 1990.
- 670 Binh, D. Van, Wietlisbach, B., Kantoush, S., Loc, H. H., Park, E., Cesare, G. de, Cuong, D. H., Tung, N. X., and Sumi, T.: A Novel Method for River Bank Detection from Landsat Satellite Data: A Case Study in the Vietnamese Mekong Delta, *Remote Sens.*, 12, <https://doi.org/10.3390/rs12203298>, 2020.
- Bracken, L. J., Turnbull, L., Wainwright, J., and Bogaart, P.: Sediment connectivity: A framework for understanding sediment transfer at multiple scales, *Earth Surf. Process. Landforms*, <https://doi.org/10.1002/esp.3635>, 2015.
- 675 Brandt, S. A.: Classification of geomorphological effects downstream of dams, *CATENA*, 40, 375–401, [https://doi.org/10.1016/S0341-8162\(00\)00093-X](https://doi.org/10.1016/S0341-8162(00)00093-X), 2000.
- Bujakowski, F. and Falkowski, T.: Hydrogeological analysis supported by remote sensing methods as a tool for assessing the safety of embankments (case study from Vistula River valley, Poland), *Water (Switzerland)*, 11, <https://doi.org/10.3390/w11020266>, 2019.
- 680 Chadwick, A. J., Greenberg, E., and Ganti, V.: Remote Sensing of Riverbank Migration Using Particle Image Velocimetry, *J. Geophys. Res. Earth Surf.*, 128, <https://doi.org/10.1029/2023JF007177>, 2023.
- Chalov, S., Ivanov, V., Danila, S., Pavlyukevich, E., Habel, M., Botavin, D., Chalova, A., Golovlev, P., Kamyshev, A., Kolesnikov, R., Koneva, U., Kurakova, A., Mikhailova, N., Tuzova, E., Prokopeva, K., Zavadsky, A., Acharyya, R., Chalov, R., Varenov, A., D.: Multi-tool dataset on Northern Eurasian Riverbank Migration (NERM) [Data set],
- 685 <https://doi.org/10.5281/zenodo.11072920>, 2024.
- Chalov, R. S. and Shkolnyi, D.: Extreme and specific manifestations of channel processes: Concepts, classifications, assessment criteria, *Izv. Ross. Akad. Nauk. Seriya Geogr.*, 31–41, <https://doi.org/10.7868/S2587556618010034>, 2018.
- Chalov, S. and Ivanov, V.: Catchment and in-channel sources in three large Eurasian Arctic rivers: Combining monitoring, remote sensing and modelling data to construct Ob', Yenisey and Lena rivers sediment budget, *CATENA*, 230, 107212,
- 690 <https://doi.org/10.1016/j.catena.2023.107212>, 2023.
- Chalov, S., Prokopeva, K., Magritsky, D., Grigoriev, V., Fingert, E., Habel, M., Juhls, B., Morgenstern, A., Overduin, P. P., and Kasimov, N.: Climate change impacts on streamflow, sediment load and carbon fluxes in the Lena River delta, *Ecol. Indic.*, 157, <https://doi.org/10.1016/j.ecolind.2023.111252>, 2023a.
- Chalov, S. R., Liu, S., Chalov, R. S., Chalova, E. R., Chernov, A. V., Promakhova, E. V., Berkovitch, K. M., Chalova, A. S.,
- 695 Zavadsky, A. S., and Mikhailova, N.: Environmental and human impacts on sediment transport of the largest Asian rivers of Russia and China, *Environ. Earth Sci.*, 77, 1–14, <https://doi.org/10.1007/s12665-018-7448-9>, 2018.
- Chalov, S. R., Chalova, A. S., and Shkolnyi, D. I.: Quantitative Assessment of Channel Planform Changes of the Kamchatka River, *Izv. Ross. Akad. Nauk. Seriya Geogr.*, 85, <https://doi.org/10.31857/S2587556621020035>, 2021.
- Chalov, S. R., Prokopeva, K. N., Shkolnyi, D. I., and Tsyplenkov, A. S.: Assessment of the Impact of Open-Cast Mining on
- 700 the Vyvenka River Basin (Kamchatka Krai), *Bull. Irkutsk State Univ. Ser. Earth Sci.*, 45, 127–149, <https://doi.org/10.26516/2073-3402.2023.45.127>, 2023b.



- Donovan, M. and Belmont, P.: Timescale dependence in river channel migration measurements, *Earth Surf. Process. Landforms*, 44, <https://doi.org/10.1002/esp.4590>, 2019.
- 705 Feyisa, G. L., Meilby, H., Fensholt, R., and Proud, S. R.: Automated Water Extraction Index: A new technique for surface water mapping using Landsat imagery, *Remote Sens. Environ.*, 140, 23–35, <https://doi.org/https://doi.org/10.1016/j.rse.2013.08.029>, 2014.
- Fuchs, M., Nitze, I., Strauss, J., Günther, F., Wetterich, S., Kizyakov, A., Fritz, M., Opel, T., Grigoriev, M. N., Maksimov, G. T., and Grosse, G.: Rapid Fluvio-Thermal Erosion of a Yedoma Permafrost Cliff in the Lena River Delta, *Front. Earth Sci.*, 8, <https://doi.org/10.3389/feart.2020.00336>, 2020.
- 710 Fuller, I. C., Large, A. R. G., and Milan, D. J.: Quantifying channel development and sediment transfer following chute cutoff in a wandering gravel-bed river, *Geomorphology*, [https://doi.org/10.1016/S0169-555X\(02\)00374-4](https://doi.org/10.1016/S0169-555X(02)00374-4), 2003.
- Gautier, E., Dépret, T., Caverro, J., Costard, F., Virmoux, C., Fedorov, A., Konstantinov, P., Jammot, M., and Brunstein, D.: Fifty-year dynamics of the Lena River islands (Russia): Spatio-temporal pattern of large periglacial anabranching river and influence of climate change, *Sci. Total Environ.*, 783, <https://doi.org/10.1016/j.scitotenv.2021.147020>, 2021.
- 715 Gelfan, A., Gustafsson, D., Motovilov, Y., Arheimer, B., Kalugin, A., Krylenko, I., and Lavrenov, A.: Climate change impact on the water regime of two great Arctic rivers: modeling and uncertainty issues, *Clim. Change*, 141, 499–515, <https://doi.org/10.1007/s10584-016-1710-5>, 2017.
- Gómez-Pazo, A., Payo, A., Paz-Delgado, M., and Delgadillo Calzadilla, M. A.: Open Digital Shoreline Analysis System: ODSAS v1.0, *J. Mar. Sci. Eng.*, 10, 26, <https://doi.org/10.3390/jmse10010026>, 2021.
- 720 Greenberg, E., Chadwick, A. J., and Ganti, V.: A Generalized Area-Based Framework to Quantify River Mobility From Remotely Sensed Imagery, *J. Geophys. Res. Earth Surf.*, 128, <https://doi.org/10.1029/2023JF007189>, 2023.
- Guy, H. P., Simons, D. B., and Richardson, E. V.: Summary of Alluvial Channel Data From Flume Experiments , 1956-61, *U.S. Geol. Surv.*, 1–104, 1966.
- Huang, C., Chen, Y., Zhang, S., and Wu, J.: Detecting, Extracting, and Monitoring Surface Water From Space Using Optical
725 Sensors: A Review, *Rev. Geophys.*, 56, 333–360, <https://doi.org/https://doi.org/10.1029/2018RG000598>, 2018.
- Ielpi, A. and Lapôtre, M. G. A.: A tenfold slowdown in river meander migration driven by plant life, *Nat. Geosci.*, 13, <https://doi.org/10.1038/s41561-019-0491-7>, 2020.
- Karashev, A. V.: Theory and methods of calculation of river sediments, *Hydrometeo.*, Leningrad, 271 pp., 1977.
- Kizyakov, A. I., Korotaev, M. V., Wetterich, S., Opel, T., Pravikova, N. V., Fritz, M., Lupachev, A. V., Günther, F., Shepelev,
730 A. G., Syromyatnikov, I. I., Fedorov, A. N., Zimin, M. V., and Grosse, G.: Characterizing Batagay megaslump topography dynamics and matter fluxes at high spatial resolution using a multidisciplinary approach of permafrost field observations, remote sensing and 3D geological modeling, *Geomorphology*, 455, 109183, <https://doi.org/10.1016/j.geomorph.2024.109183>, 2024.
- Knighton, D.: *Fluvial Forms and Processes*, <https://doi.org/10.4324/9780203784662>, 2014.
- 735 Kronvang, B., Andersen, H., Larsen, S., and Audet, J.: Importance of bank erosion for sediment input, storage and export at



- the catchment scale, *J Soils Sediments*, 13, 230–241, <https://doi.org/10.1007/s11368-012-0597-7>, 2013.
- Kurakova, A. . and Chalov, R. S.: Coast washouts in the latitudinal section of the Middle Ob and their connection with the morphology of the riverbed, *Geogr. Bull.*, 3, 34–47, <https://doi.org/10.17072/2079-7877-2019-3-34-47>, 2019.
- Langhorst, T. and Pavelsky, T.: Global Observations of Riverbank Erosion and Accretion From Landsat Imagery, *J. Geophys. Res. Earth Surf.*, 128, <https://doi.org/10.1029/2022JF006774>, 2023.
- 740 Laonamsai, J., Julphunthong, P., Saprathet, T., Kimmany, B., Ganchanasuragit, T., Chomcheawchan, P., and Tomun, N.: Utilizing NDWI, MNDWI, SAVI, WRI, and AWEI for Estimating Erosion and Deposition in Ping River in Thailand, *Hydrology*, 10, <https://doi.org/10.3390/hydrology10030070>, 2023.
- Lappalainen, H. K., Altimir, N., Kerminen, V.-M., Petäjä, T., Makkonen, R., Alekseychik, P., Zaitseva, N., Bashmakova, I.,
745 Kujansuu, J., Lauri, A., Haapanala, P., Mazon, S. B., Borisova, A., Konstantinov, P., Chalov, S., Laurila, T., Asmi, E., Lihavainen, H., Bäck, J., Arshinov, M., Mahura, A., Arnold, S., Vihma, T., Uotila, P., De Leeuw, G., Kukkonen, I., Malkhazova, S., Tynkkynen, V.-P., Fedorova, I., Hansson, H. C., Dobrolyubov, S., Melnikov, V., Matvienko, G., Baklanov, A., Viisanen, Y., Kasimov, N., Guo, H., Bondur, V., Zilitinkevich, S., and Kulmala, M.: PAN-EURASIAN EXPERIMENT (PEEX) PROGRAM: AN OVERVIEW OF THE FIRST 5 YEARS IN OPERATION AND FUTURE PROSPECTS, *Geogr.*
750 *Environ. Sustain.*, 11, 6–19, <https://doi.org/10.24057/2071-9388-2018-11-1-6-19>, 2018.
- de Lima, L., Fernández-Fernández, S., Espinoza, J., da Guia Albuquerque, M., and Bernardes, C.: End point rate tool for QGIS (EPR4Q): Validation using DSAS and AMBUR, *Int. J. Geo-Information*, 10, 162, <https://doi.org/10.3390/ijgi10030162>, 2021.
- Linke, S., Lehner, B., Ouellet Dallaire, C., Ariwi, J., Grill, G., Anand, M., Beames, P., Burchard-Levine, V., Maxwell, S., Moidu, H., Tan, F., and Thieme, M.: Global hydro-environmental sub-basin and river reach characteristics at high spatial
755 resolution, *Sci. data*, <https://doi.org/10.1038/s41597-019-0300-6>, 2019.
- Liu, H., Hu, H., Liu, X., Jiang, H., Liu, W., and Yin, X.: A Comparison of Different Water Indices and Band Downscaling Methods for Water Bodies Mapping from Sentinel-2 Imagery at 10-M Resolution, *Water*, 14, <https://doi.org/10.3390/w14172696>, 2022.
- Mandarino, A., Maerker, M., and Firpo, M.: Channel planform changes along the Scrivia River floodplain reach in northwest
760 Italy from 1878 to 2016, in: *Quaternary Research (United States)*, 1–18, <https://doi.org/10.1017/qua.2018.67>, 2019.
- Morin, P., Porter, C., Cloutier, M., Howat, I., Noh, M.-J., Willis, M., Bates, B., Williamson, C., and Peterman, K.: ArcticDEM: A Publicly Available, High Resolution Elevation Model of the Arctic, in: *EGU General Assembly Conference Abstracts*, EPSC2016-8396, 2016.
- Murton, J. B., Goslar, T., Edwards, M. E., Bateman, M. D., Danilov, P. P., Savvinov, G. N., Gubin, S. V., Ghaleb, B., Haile,
765 J., Kanevskiy, M., Lozhkin, A. V., Lupachev, A. V., Murton, D. K., Shur, Y., Tikhonov, A., Vasil'chuk, A. C., Vasil'chuk, Y. K., and Wolfe, S. A.: Palaeoenvironmental Interpretation of Yedoma Silt (Ice Complex) Deposition as Cold-Climate Loess, *Duvanny Yar, Northeast Siberia, Permafrost Process.*, 26, 208–288, <https://doi.org/10.1002/ppp.1843>, 2015.
- Musie, W. and Gonfa, G.: Fresh water resource, scarcity, water salinity challenges and possible remedies: A review, *Heliyon*, 9, e18685, <https://doi.org/10.1016/j.heliyon.2023.e18685>, 2023.



- 770 Obu, J., Westermann, S., Bartsch, A., Berdnikov, N., Christiansen, H. H., Dashtseren, A., Delaloye, R., Elberling, B., Etzelmüller, B., Kholodov, A., Khomutov, A., Kääb, A., Leibman, M. O., Lewkowitz, A. G., Panda, S. K., Romanovsky, V., Way, R. G., Westergaard-Nielsen, A., Wu, T., Yamkhin, J., and Zou, D.: Northern Hemisphere permafrost map based on TTOP modelling for 2000–2016 at 1 km² scale, <https://doi.org/10.1016/j.earscirev.2019.04.023>, 2019.
- Payne, C., Panda, S., and Prakash, A.: Remote Sensing of River Erosion on the Colville River, North Slope Alaska, *Remote Sens.*, 10, <https://doi.org/10.3390/rs10030397>, 2018.
- 775 Peel, M. C., Finlayson, B. L., and McMahon, T. A.: Updated world map of the Köppen-Geiger climate classification, *Hydrol. Earth Syst. Sci.*, 11, <https://doi.org/10.5194/hess-11-1633-2007>, 2007.
- Pekel, J.-F., Cottam, A., Gorelick, N., and Belward, A. S.: Global Surface Water Explorer, 2016, 2016.
- Pickens, A. H., Hansen, M. C., Hancher, M., Stehman, S. V., Tyukavina, A., Potapov, P., Marroquin, B., and Sherani, Z.:
- 780 Mapping and sampling to characterize global inland water dynamics from 1999 to 2018 with full Landsat time-series, *Remote Sens. Environ.*, 243, 111792, <https://doi.org/10.1016/j.rse.2020.111792>, 2020.
- Piégay, H., Arnaud, F., Belletti, B., Bertrand, M., Bizzi, S., Carbonneau, P., Dufour, S., Liébault, F., Ruiz-Villanueva, V., and Slater, L.: Remotely sensed rivers in the Anthropocene: state of the art and prospects, *Earth Surf. Process. Landforms*, 45, 157–188, <https://doi.org/https://doi.org/10.1002/esp.4787>, 2020.
- 785 Reid, L. M. and Dunne, T.: Sediment budgets as an organizing framework in fluvial geomorphology, in: *Tools in Fluvial Geomorphology*, Wiley, 357–380, <https://doi.org/10.1002/9781118648551.ch16>, 2016.
- Rowland, J. C., Jones, C. E., Altmann, G., Bryan, R., Crosby, B. T., Geernaert, G. L., Hinzman, L. D., Kane, D. L., Lawrence, D. M., Mancino, A., Marsh, P., McNamara, J. P., Romanovsky, V. E., Toniolo, H., Travis, B. J., Trochim, E., and Wilson, C. J.: Arctic landscapes in transition: Responses to thawing permafrost, *Eos (Washington. DC.)*, 91,
- 790 <https://doi.org/10.1029/2010EO260001>, 2010.
- Rowland, J. C., Shelef, E., Pope, P. A., Muss, J., Gangodagamage, C., Brumby, S. P., and Wilson, C. J.: A morphology independent methodology for quantifying planview river change and characteristics from remotely sensed imagery, *Remote Sens. Environ.*, 184, 212–228, <https://doi.org/10.1016/J.RSE.2016.07.005>, 2016.
- Rowland, J. C., Schwenk, J. P., Shelef, E., Muss, J., Ahrens, D., Stauffer, S., Pilliouras, A., Crosby, B., Chadwick, A., Douglas,
- 795 M. M., Kemeny, P. C., Lamb, M. P., Li, G. K., and Vulis, L.: Scale-Dependent Influence of Permafrost on Riverbank Erosion Rates, *J. Geophys. Res. Earth Surf.*, 128, <https://doi.org/10.1029/2023JF007101>, 2023.
- Saunders, A. D., England, R. W., Reichow, M. K., and White, R. V.: A mantle plume origin for the Siberian traps: Uplift and extension in the West Siberian Basin, Russia, *Lithos*, 79, <https://doi.org/10.1016/j.lithos.2004.09.010>, 2005.
- Sidorchuk, A.: The Potential of Gully Erosion on the Yamal Peninsula, West Siberia, *Sustainability*, 12, 260,
- 800 <https://doi.org/10.3390/su12010260>, 2019.
- Strauss, J., Laboor, S., Schirrmeyer, L., Fedorov, A. N., Fortier, D., Froese, D., Fuchs, M., Günther, F., Grigoriev, M., Harden, J., Hugelius, G., Jongejans, L. L., Kanevskiy, M., Kholodov, A., Kunitsky, V., Kraev, G., Lozhkin, A., Rivkina, E., Shur, Y., Siegert, C., Spektor, V., Streletskaia, I., Ulrich, M., Vartanyan, S., Veremeeva, A., Anthony, K. W., Wetterich, S., Zimov, N.,



- and Grosse, G.: Circum-Arctic Map of the Yedoma Permafrost Domain, *Front. Earth Sci.*, 9, 1–15,
805 <https://doi.org/10.3389/feart.2021.758360>, 2021.
- Sylvester, Z., Durkin, P., and Covault, J. A.: High curvatures drive river meandering, *Geology*, 47, 263–266,
<https://doi.org/10.1130/G45608.1>, 2019.
- Szumińska, D., Koziół, K., Chalov, S. R., Efimov, V. A., Frankowski, M., Lehmann-Konera, S., and Polkowska, Ż.:
810 Reemission of inorganic pollution from permafrost? A freshwater hydrochemistry study in the lower Kolyma basin (North-
East Siberia), *L. Degrad. Dev.*, 34, 5591–5605, <https://doi.org/10.1002/ldr.4866>, 2023.
- Thorne, C. R.: Field measurements of rates of bank erosion and bank material strength., *Eros. sediment Transp. Meas. Proc.*
Florence Symp. June 1981, (International Assoc. Hydrol. Sci. IAHS-AISH Publ. 512), 1981.
- Wilkinson, S., Prosser, I., Rustomji, P., and Read, A.: Modelling and Testing Spatially Distributed Sediment Budgets to
Related Erosion Processes to Sediment Yields, *Environ. Model. Softw.*, 24, 489–501,
815 <https://doi.org/10.1016/j.envsoft.2008.09.006>, 2009.
- Zhou, Y., Dong, J., Xiao, X., Xiao, T., Yang, Z., Zhao, G., Zou, Z., and Qin, Y.: Open Surface Water Mapping Algorithms: A
Comparison of Water-Related Spectral Indices and Sensors, *Water*, 9, <https://doi.org/10.3390/w9040256>, 2017.